Nephelauxetic effect of low phonon antimony oxide glass in absorption and photoluminescence of rare-earth ions

Tirtha Som, Basudeb Karmakar*

Glass Science and Technology Section, Glass Division,
Central Glass and Ceramic Research Institute (CSIR, India),
196 Raja S. C. Mullick Road, Kolkata 700 032, West Bengal, India

---

Abstract

An antimony oxide based monolithic glass with very high Sb_2O_3 content (70 mol%) in the system K_2O-B_2O_3-Sb_2O_3 (KBS) has been prepared for the first time. Its phonon energy (602 cm^{-1}), evaluated by infrared reflection spectroscopy, is found to be very close to that of fluoride glasses (500-600 cm^{-1}). After doping with different rare-earth ions, their UV-Vis absorption and photoluminescence properties have been explored, compared with those observed in other hosts and justified with quantitative calculation of nephelauxetic parameter and covalent bonding characteristics. It is been proposed that tunable laser or new color visible light sources may be obtained by controlling these fundamental properties of the glass host. The results also suggest that KBS glass may be used as hosts in the place of fluoride glasses. The Judd-Ofelt parameters, $\Omega_{t=2,4,6}$ for Nd^{3+}, Ho^{3+}, and Er^{3+} doped in KBS glass have been evaluated and compared with other glasses. It is established that $\Omega_{t=2}$ value follow a direct relationship with covalent character of the hosts which not only supports the above calculation but also provides a generalized evidence for the sensitivity of this parameter to their bonding characteristics.

Keywords: Antimony oxide glass; Rare-earth ions; Nephelauxetic effect; Judd-Ofelt parameters; Electronegativity; Covalent bonding character; Low phonon glass; Absorption; Luminescence

*Corresponding author. Tel: +91-33 2473 3469; fax: +91-33 2473 0957

E-mail address: basudebk@cgcri.res.in (B. Karmakar)

1. Introduction

Spectroscopy of the lanthanides or rare-earth ions (RE^{3+}) ions incorporated in different dielectrics (crystalline or amorphous glass host matrices) has been one of the most interesting areas of solid-state research since the first demonstration of lasing action in Nd-doped glass by Snitzer in 1961 [1]. The applications of RE^{3+} ions now extend to almost all important fields of technology. The Eu^{3+}, Tb^{3+} and Tm^{3+} ions are mainly exploited for their application in display devices due to their red, green and blue emissions respectively [2]. Photoluminescence of Nd^{3+}, Ho^{3+}, Dy^{3+} and Sm^{3+} ions are investigated for application in high-energy particle detector, biomedical lasers, optical data storage, bar-code reading, laser printing, underwater and satellite communication, environment friendly solid-state lighting, etc [2-5] while Pr^{3+}, Nd^{3+}, Dy^{3+}, Er^{3+} and Tm^{3+} ions to develop fiber amplifiers in the optical communication transmission system, eye-safe lasers, luminescent solar concentrators, etc. [2,6]. Except for Pm and Gd, all of the lanthanide ions has transitions that are useful for many solid state laser and integrated photonics applications.

Although the 4f electrons of RE^{3+} ions are shielded by the 5s and 5p electrons, the spin–orbit interactions (depending on the number of 4f electrons) exert much influence on the positions of their electronic energy levels. The characteristic emission properties of different RE^{3+} ions ultimately arise due to electronic transitions between these energy levels. The surrounding ligand-field or the host matrix incorporating the RE^{3+} ions also exerts a considerable influence on the lasing properties [7,8]. Therefore, the spectroscopic behavior of any trivalent rare earth ion will be dissimilar in different hosts [7] and has to be judiciously utilized for various applications.

Initially, investigation of glasses as host materials for RE photoluminescence was confined to the conventional glass formers like silicates, borates, and phosphates [4,7-9]. In the 1980's, RE^{3+}-doped fluoride glasses as active laser hosts were a major breakthrough [10]. Heavy metal fluoride glass (HMFG, ZBLAN, etc.) as hosts for RE^{3+} dopants was found to provide additional benefits, in contrast to conventional silicate, borate and phosphate glasses, due to their significantly low phonon energy or resonance vibration of the matrix (500-600 cm^{-1}), high capability to incorporate large amount of RE dopants which provides the freedom to tailor the dopant concentration for specific applications, and extended transparency from the near-UV to the mid-IR region [11-15]. Because radiative emissions are more efficient in fluoride glasses due to their lower phonon energies, the large number of laser transitions observed for different RE^{3+} ions in ZBLANP fluoride glass has been demonstrated and summarized by France [11].

But fluoride glasses endure some serious limitations. The weak nature of the chemical bonds leads to mechanical weakness, lower temperature stability, devitrification and difficulty in preparation [10,11,16]. Iqbal et al [16] demonstrated melting of 20g fluoride glass batches in platinum crucibles in a glove-box environment where moisture and oxygen levels were kept below 1 ppm. On the contrary, heavy metal oxide glasses (HMO) exhibit better thermal, mechanical and chemical durability than fluoride glasses. Their melting does not require any sophisticated apparatus (can be melted in ambient atmosphere). The desire for low phonon energy host coupled with the need to retain mechanical strength, low manufacturing temperatures and high refractive index has currently led to a plethora of studies on heavy metal oxide [17-24] and heavy metal oxyfluoride glasses [3,5,6,25-27]. Several comparative spectroscopic studies of the RE-

doped heavy metal oxide, fluoride as well as oxy-fluoride glasses have been made not only in relation to the practical applications of these optical materials as laser active media, optical waveguides and infrared-to-visible up-converters, but also to their ease of preparation, feasibility of application and stability against atmosphere moisture [28,29].

In recent years considerable emphasis has been given to the discovery of new HMO glass compositions for exploitation as RE-doped luminescent hosts. The characteristic properties of HMO glasses that make them attractive for device fabrication are related to their relatively high refractive index, high dispersion, low melting temperatures, wide transmission window, and low phonon energy (lattice vibrations of the material) among oxide glass formers [30]. The reduced phonon energy increases the efficiency of luminescence from excited states of RE^{3+} ions in these matrices and provides the possibility to develop more efficient visible optical lasers. The development of a new HMO based glass system having phonon energy comparable to that of fluoride glass was a challenge to the scientific community.

Among the HMO glasses, tellurite, lead, bismuth and germanate glasses have been the subjected to several investigations for their potential as laser host matrices [2,3,5,6,17-28]. But there are only a few of investigations of RE^{3+}-doped unusual antimony(III) oxide glasses. This is due to several difficulties of their preparation in the bulk monolithic form owing to the high volatility of the melts, intense crystallization during cooling, and also Sb_2O_3 inadequately forms the glass network due to its low field strength of Sb^{3+} (0.73) [30]. Application of forced cooling or quenching techniques do yield high antimony containing glasses but usually as tiny pieces incompatible for real photonic applications [31]. Recently, Sudhakar et al. [32] and Qian et al. [33] have

reported the fluorescence properties of Tm^{3+} and Er^{3+} in glasses containing about 20-40 mol% Sb_2O_3. But to the best of our knowledge there is no report of photoluminescence of RE^{3+} ions in Sb_2O_3 -based glasses, that is, glasses comprising of 50 mol% or more of Sb_2O_3 before us [34-36]. Theoretically antimony glasses are expected to possess low phonon energy (about 600 cm^{-1}) due to low stretching vibration of Sb-O-Sb bond [37]. By careful selection of melting temperature and glass composition, lately we synthesized monolithic antimony oxide glasses [31] and demonstrated that glasses containing 70 mol% Sb_2O_3 exhibited remarkable upconversion properties of Sm^{3+}, Nd^{3+} and Er^{3+} ions [34-36]. Qian et al. [33] also showed that quantum efficiency $^4I_{13/2} \rightarrow {}^4I_{15/2}$ transition of Er^{3+} increases from 9.3 to 28.7% due to increase in Sb_2O_3 content in glass from 20 to 30 mol%, owing to the decrease of the multiphonon decay rate in the glass host. Therefore, monolithic Sb_2O_3-based glasses doped with RE^{3+}ions like Pr^{3+}, Eu^{3+}, Tb^{3+}, Dy^{3+}, Ho^{3+}, Tm^{3+} and Yb^{3+} ions, if synthesized, would be very attractive photoluminescent materials because of their low phonon energy. Moreover, such a systematic study is also missing in the literature.

Many fluorescent transitions of rare earth ions of practical importance are initiated from an excited level which has a small energy gap from the next level. Examples of such transitions are $^3P_0 \rightarrow {}^3F_2$ (deep-red) transition of Pr^{3+} [28], $^4S_{3/2} \rightarrow {}^4I_{15/2}$ (green) transition of Er^{3+} [35], $^5D_1 \rightarrow {}^7F_1$ (green) emission of Eu^{3+}[38], $^5F_3 \rightarrow {}^5I_8$ (blue) and ($^5S_2$, $^5F_4$) $\rightarrow {}^5I_8$ (green) emission of Ho^{3+} [17], $^1G_4 \rightarrow {}^3F_4$ (red) emission of Tm^{3+} [2], etc. Materials with lower phonon energy are required as a host to obtain these desired transitions. Again suitable disordered hosts (glasses) can be used to manipulate the various colored transitions of RE^{3+} ions, particularly yellow to blue integral intensities of

Dy^{3+} [39,40] and as well as blue-green-red ratio of Tm^{3+}/Dy^{3+} and Sm^{3+}/Tm^{3+} to develop environment friendly white light which has high potential for replacing the conventional incandescent and fluorescent lamps [41,42].

Apart from phonon energy, covalency is another very significant parameter which direct the suitability of glasses matrices for rare-earth fluorescence. Larger the oxide ion polarizability leads to larger refractive index. Consequently greater covalency results in enhancement of the transition probability. Generally the Judd–Ofelt parameter (Ω_2) is used an indication of rare-earth–ligand bond covalency, but any direct correlation of covalency (a fundamental property generally used by the chemists) and Ω_2 (a parameter generally used by the physicists) is seldom discussed. Besides, mainly two aspects, one pertaining to the variation in the Judd-Ofelt parameters as one move along the rare-earth series and the other pertaining to the influences of the host matrices on the hypersensitive transitions, are generally investigated [3,17,43]. However, the direct influence of the covalent character, which is an intrinsic fundamental property controlled by the nephelauxetic effect (or glass chemistry), on the position of the absorption bands of the RE^{3+} ions have been rarely studied.

Motivated by all these considerations and as a sequel to our previous work on spectroscopic investigations of RE-doped antimony oxide glasses [34-36], in this paper we report for the first time the photoluminescence properties of RE^{3+}ions like Pr^{3+}, Eu^{3+}, Tb^{3+}, Dy^{3+}, Ho^{3+}, Tm^{3+} and Yb^{3+} ions under UV and near-visible light excitation incorporated in high antimony oxide (70 mol%) containing $15K_2O–15B_2O_3–70Sb_2O_3$ (KBS) low phonon oxide glasses and predict their potential laser properties. Infrared reflection spectral study has been conducted to establish the low phonon energy of the

KBS glass. The effect of covalency and nephelauxetic parameter of various host on the absorption band positions are also discussed. The Judd-Ofelt parameters of the Nd^{3+}, Ho^{3+}, and Er^{3+} ions in this KBS glass have been evaluated, and the direct relationship between covalency and Ω_2 has been shown mathematically.

2. Experimental

The composition (mol %) of the KBS antimony (base) glasses is $15K_2O$-$15B_2O_3$-$70Sb_2O_3$ glasses. The raw materials were antimony(III) oxide, Sb_2O_3 (GR, 99%, Loba Chemie) and potassium metaborate, KBO_2 (Johnson Matthey) and rare-earth oxides RE_2O_3 (99.9%, Alfa Aesar). Each batch of 20 g glass comprising of appropriate amounts of the raw materials was doped individually with 0.7 wt % concentrations of RE^{3+} in excess and mixed thoroughly. This is because our preliminary experiments show that in KBS glass the maximum luminescence is obtained by doping with 0.7 wt% RE_2O_3. The RE-doped glasses were prepared following the procedure stated in our previous publications (melted in ambient atmosphere) [34-36]. Although the melting was done in high purity silica crucibles, but a small quantity SiO_2 (2-2.5 mol%) has been eluted from the crucibles by the glasses during melting. There was also about 2-4 mol% loss of Sb_2O_3 due to its volatization. The glasses obtained as round discs of diameters about 4 ± 0.5 cm and thickness about 3 ± 0.2 mm were cut into half-circular discs and polished to 2 ± 0.1 mm thickness for optical measurement.

The density was measured by the Archimedes method using toluene as the buoyancy liquid and a single pan balance, with an error of ± 0.006g.cm^{-3}, using the formula:

$$\rho = [W_a / (W_a - W_t)] \times \rho_t \qquad (1)$$

where W_a and W_t are the weight of the sample in are and toluene respectively and ρ_t is the density of toluene at the experimental temperature (25ºC) and was found to be 0.861 g.cm^{-3}. The amorphicity of the glasses were confirmed by X-ray diffraction (XRD) analysis. The infrared reflection spectrum (FT-IRRS) of the base KBS glass in the range 400-1500 cm^{-1} was recorded with a Fourier transform infrared (FTIR) spectrometer (Perkin Elmer, FTIR 1615) at an incident angle of 15º and with the help of a specular reflectance attachment at the resolution of ±1 cm^{-1} and after 256 scans. The UV-Vis absorption spectra of polished samples of thickness 2 ± 0.1 mm were obtained with a double-beam spectrophotometer (Perkin Elmer, Lambda 20) at an error of ± 0.1 nm in band position. Fluorescence spectra were measured, at an error of ± 0.2 nm, with a fluorescence spectrophotometer (Spex, Fluorolog 2) in which a xenon discharge lamp (150 W) was used as the excitation source. The absorption and fluorescence spectrophotometers were calibrated using standard Ho^{3+} ion doped samples supplied by the manufacturer of the instruments and the discrepancy in peak position was found to be within an error of ± 0.1 and ± 0.2 nm respectively. Excitation of different parts of the same sample yielded similar luminescence spectra with ± 1% error intensity in peak intensity. This emphasizes the homogeneity of the RE-doped antimony glasses. All the measurements were carried out at room temperature.

3. Results and discussion

3.1 Phonon energy of KBS glass

The infrared reflection spectra (IRRS) [32,44,45], which represent the total vibrations of the whole matrix, is one of the alternative ways to measure the phonon energy (ħω) of glasses besides phonon side band (PSB) [46,47] and Raman spectra [48-51]. The average ħω values obtained by each of these methods are very close to each other. In the case of the IRRS which is generally recorded in the ~ 400-1500 cm^{-1} region, the wavenumber at the highest intensity main peak is cited as the phonon energy of the glass matrix [32,44,45]. The IRRS of KBS glass in the region 490-1500 cm^{-1} is displayed in Fig. 1. Two major reflection bands centered at 602 and 1207 cm^{-1} are observed. The highest intensity main reflection band centered at 602 cm^{-1} arises due to Sb-O-Sb stretching vibration [32,37] while the other one at 1207 cm^{-1} is due to B-O-B stretching vibration of $[BO_3]$ unit [32]. We have denoted the major and maximum intensity Sb-O-Sb stretching band at 602 cm^{-1} as the phonon energy of KBS antimony oxide glass.

The apparent formation of the Sb-O-B bonds is clearly reflected in the IRRS for the series of KBS glasses having composition (mol%) xK_2O-xB_2O_3-$(100 - 2x)Sb_2O_3$, where x = 5–35 [31] where with decrease in borate content, there is a blue shift of the $[BO_3]_3$ stretching vibration band from 1207 to 1187 cm^{-1}. This indicates formation of Sb-O-B more linkages. The apparent shift towards lower wavenumber is due to contributions from heavier Sb atom. Although Sb^{3+} (as Sb_2O_3) has been used as the raw material, but due to the multivalent characteristics of Sb, it is expected that during the melting at high temperature (900ºC) in ambient atmosphere, a small part of Sb^{3+} is transformed into Sb^{5+} (Sb_2O_5) state by accepting oxygen from air [31]. These Sb^{5+} ions enter into the glass as

singly positive [SbO_4] 4-coordinated units [31]. Absence of any metallic species of Sb was confirmed by absence of any peaks in the XRD spectra. The luminescence spectra of the mother glass showed no bands which could be attributed to Sb clusters.

In Table 1, the phonon energy of KBS antimony oxide glass host is compared with several other hosts [44-55]. The phonon energy of KBS glass is considerably less than those of borate, phosphate, silicate, germanate and even tellurites glasses and is close to that of fluoride glass. The phonon energy of isolated O-H bond is at 3500 cm^{-1} and that of the aqua ions is usually considered to be 3200 cm^{-1} [55] due to the stretching vibration of O-H bonds and hydrogen bonded hydroxyl groups ($-O-H^{\delta+}\ldots O^{\delta-}$) respectively. In case of the KBS antimony glass, there is sharp band at 3259 cm^{-1} due to hydrogen bonded hydroxyl groups ($–O–H^{\delta+}----O^{\delta–}$) [31]. The OH content in the KBS glass has been estimated to be 133 ppm [31,35].

3.2 Praseodymium, Pr^{3+} ($4f^2$)

The absorption spectrum of Pr^{3+}-doped antimony glass is featured in Fig. 2(a). A total of 4 absorption bands are observed to arise from the ground $^3H_4$ state. The absorption bands at 445.7, 472.3, 485.3 and 593.5 nm ascribed to $^3H_4 \rightarrow {}^3P_2$, $^3H_4 \rightarrow {}^3P_1$, $^3H_4 \rightarrow {}^3P_0$, and $^3H_4 \rightarrow {}^1D_2$ electric-dipole transitions in Pr^{3+} ion respectively [56]. The complex group of transitions from the $^3H_4$ to the excited-state $^3P_{J(J=0,1,2)}$ multiplets in violet-blue attributes blue color to the Pr^{3+} ion. But the present Pr^{3+}-doped KBS antimony glass is green in color. The observed color is due to the combined effect of f→f transitions and transition between HOMO (Sb 5s + O 2p) and LUMO (Sb 5p) in Sb_2O_3 which imparts yellow color to the undoped base glass. The associated transitions in

comparison to those in ZBLANP fluoride glass (mol % $51.5ZrF_4$-$19.5BaF_2$-$5.3LaF_3$-$3.2AlF_3$-$18NaF$-$2.5PbF_2$) [11], InF_3-based heavy metal fluoride glass, IZBSGL (mol % $45InF_3$–$14ZnF_2$–$19BaF_2$–$17SrF_2$–$3GaF_3$–$2LaF_3$) [27], aqueous solution (mol% $100H_2O$) [56] and PbO-based heavy metal oxide glasses PTO (mol % $70PbO$-$30TiO_2$) [17] and PGO (mol % $60PbO$-$40GeO_2$) [57] glass are provided in Table 2 to correlate absorption band position with nephelauxetic parameter (β) and covalent bonding properties of the host (C_{cov} %).

Figure 2(b) presents the emission spectrum of Pr^{3+} ions using the 446 nm excitation wavelength. A very strong emission band due to $^3P_0 \rightarrow {}^3H_6$ and $^3P_1 \rightarrow {}^3F_2$ transitions is observed at 607 nm having a FWHM of about 29 nm. Two strong bands are also obtained at 532.5 and 652 nm due to $^3P_0 \rightarrow {}^3H_5$ and $^3P_0 \rightarrow {}^3F_2$ transitions respectively. In addition series of weak emission bands are also obtained at 678 ($^3P_1 \rightarrow {}^3F_3$), 694 ($^3P_1 \rightarrow {}^3F_4$ and $^3P_0 \rightarrow {}^3F_3$) and 717 nm ($^3P_0 \rightarrow {}^3F_4$) respectively. Similar emission bands (not shown here) are also obtained with 473 and 485 excitation wavelengths. The position of the emissions wavelengths of Pr^{3+} ion in KBS glass is compared with those obtained in ZBLANP [11], IZBSGL [27], PTO [17] and GNK (mol % $50GeO_2$–$25Nb_2O_5$–$25K_2O$) [58] glasses in Table 3. Although the capacity of incorporating RE^{3+} ions by different glass host may be widely different but the quantity of RE^{3+} does not exert any influence on the position of absorption and emission bands.

Under 446 nm excitation, the Pr^{3+} ions are first excited to $^3P_2$ level from which multiphonon relaxation takes place mainly resulting in the population of the $^3P_1$ and $^3P_0$ levels. Earlier from the infrared reflection study (see Fig. 1), we have established that the phonon energy of this KBS glass is about 602 cm^{-1}. Due to the large energy gap (~3757

cm^{-1}) between $^3P_0$ and $^1D_2$ and the low phonon energy (602 cm^{-1}), non-radiative multiphonon relaxation from $^3P_0$ to $^1D_2$ is very small, and hence luminescence the $^1D_2$ level was not observed. The rate of multiphonon relaxation process (W_p) may be expressed by the Miyakawa-Dexter equation as [59]:

$$W_p = W_p(0) \exp(-\alpha \Delta E/\hbar\omega) \quad (2)$$

$$\alpha = \ln\{p/g[n(t) + 1]\} - 1 \quad (3)$$

$$p \approx \Delta E / \hbar\omega \quad (4)$$

where g is the electron-phonon coupling constant, ΔE is the energy gap between two energy levels (7935 cm^{-1}), $\hbar\omega$ is the phonon energy of the glass host and p is phonon numbers needed for multiphonon relaxation. Hence a minimum of six photons (calculated $p = 6$) are required for bridging the $^3P_0 \rightarrow {}^1D_2$ multiphonon relaxation process where as only one and two photons are required to bridge the energy gap between $^3P_2 \rightarrow {}^3P_1$ (~ 1267 cm^{-1}) and $^3P_1 \rightarrow {}^3P_0$ (~507 cm^{-1}) respectively. The W_p decreases strongly with increasing in p according to Eq. (3). Thus the populations of the metastable $^3P_1$ and $^3P_0$ levels are highly increased leading to green and intense red transitions and some emissions in the NIR region as well in contrast to those in high phonon energy glasses [8]. The high phonon orders (phonons ≥ 3) due to the low phonon energy of the glass host which decreases the possibility of non-radiative multiphonon bridging and consequently manifests the multi-channel emission processes.

3.3 Europium, Eu^{3+} ($4f^6$)

The ultraviolet-visible (UV-Vis) absorption spectrum of the 0.7 wt% Eu_2O_3 doped antimony glass is depicted in Fig. 3(a). A total of five absorption bands originating due to

$^7F_0 \rightarrow {}^5L_6$, $^7F_1 \rightarrow {}^5D_3$, $^7F_0 \rightarrow {}^5D_2$, $^7F_0 \rightarrow {}^5D_1$ and $^7F_1 \rightarrow {}^5D_1$ are observed. The frequency of the absorption bands in comparison to those in ZBLANP fluoride glass [11], tellurite-based TL (mol % $80TeO_2$-$20Li_2CO_3$) glass [60], aqueous solution [61] and bismuth-based BPAWE (mol % $10B_2O_3$-$80PbO$-$6Al_2O_3$-$3WO_3$-$1Eu_2O_3$) [18] glass are provided in Table 2. The fluorescence spectrum of Eu^{3+} doped antimony glasses is shown in Fig. 3(b). The emission spectra consist of a series of six emissions bands situated at about 536 (green), 582 (yellow), 595 (orange), 617 (red), 656 (deep-red) and 705 (deep-red) nm. These bands originate due to $^5D_1 \rightarrow {}^7F_1$, $^5D_0 \rightarrow {}^7F_0$, $^5D_0 \rightarrow {}^7F_1$, $^5D_0 \rightarrow {}^7F_2$, $^5D_0 \rightarrow {}^7F_3$ and $^5D_0 \rightarrow {}^7F_4$ electronic transitions respectively. The Eu^{3+}emissions wavelengths in KBS glass are compared with those obtained in ZBLANP [11], tellurite-based TL [60] and GTK (mol % $60GeO_2$–$20TiO_2$–$20K_2O$) [2] glasses.

The ratio of integrated intensities of the hypersensitive electric dipole transition $^5D_0 \rightarrow {}^7F_2$ (red emission; ΔJ=2) over the less-sensitive magnetic dipole $^5D_0 \rightarrow {}^7F_1$ (orange emission; ΔJ=1) is commonly used as a measure of the asymmetry around the rare earth sites as well as covalency of Eu^{3+}—ligand bond [17]. The ratio, R varies from 1.3 in heavy metal fluoride glass (composition: mol % $60ZrF_4$–$33BaF_2$–$6LaF_3$–$1EuF_3$) to 7.04 in phosphate glass (composition: mol % $49.5P_2O_5$–$49.5MgO$–$1Eu_2O_3$) [60]. The value of R in KBS antimony glass is 2.9. The ratio also provides valuable information about the red color enrichment compared to the orange emission in developing strongly red luminescent optical systems. The existence of the strong green emission due to $^5D_1 \rightarrow {}^7F_1$ transition is a direct evidence of the low phonon energy of the KBS host [38]. A comparison of the emission wavelengths of Eu^{3+} of with covalent character of the host is made in Table 4.

3.4 Terbium, Tb^{3+} ($4f^8$)

The ground state of the Tb^{3+} ion is $^7F_6$. Generally Tb^{3+} doped glasses show very poor absorption spectra. However, they give an intense fluorescence in the green region [2,4,8,11]. In the absorption spectra of the Tb^{3+}-doped glass we observe a weak absorption band at 485.8 nm due to $^7F_6 \rightarrow {}^5D_4$ electronic transition (Fig. 4a and Table 2) [62]. Figure 4(b) shows the emission spectra of 0.7wt % Tb^{3+} singly doped glasses. From emission spectra, three emission transitions, $^5D_4 \rightarrow {}^7F_5$ (547 nm, strong green, FWHM = 11 nm), $^5D_4 \rightarrow {}^7F_4$ (587 nm, medium orange, FWHM = 15 nm) and $^5D_4 \rightarrow {}^7F_3$ (626 nm, medium deep-red, FWHM = 11 nm) have been identified. Their positions have been compared with the ZBLANP [11], silica based SALG (mol % $50SiO_2$–$20Al_2O_3$–$10Li_2O$–$20GdF_3$) [42], GeO_2 based GTK (mol % $60GeO_2$–$20TiO_2$–$20K_2O$) [2] and phosphate based PAKB (mol % $60P_2O_5$-$10Al_2O_3$-$20K_2O$-10BaO) [63] glasses in Table 3.

When excited by 486 nm excitation wavelength, the $^5D_4$ levels of Tb^{3+} are populated. Due to the large difference between this level and the next $^7F_0$ level (ΔE = 14800 cm^{-1}) combined with the low phonon energy of the glass, multiphonon relaxation from the $^4D_4$ level to $^7F_0$ level does not take place as 25 photons are required to bridge the gap by multiphonon relaxation. Consequently, the population of the $^5D_4$ level is expected to increase tremendously owing to the low phonon effect of the glass and thereby leading to intense green emission despite the fact that the 547 nm ($^5D_4 \rightarrow {}^7F_5$) green emission is Laporte-forbidden one obeying the MD selection rule of $\Delta J = \pm 1$ [2].

3.5 Dysprosium, Dy^{3+} ($4f^9$)

Figure 5(a) shows the absorption spectrum of the Dy^{3+}-doped antimony glass. Six absorption bands are observed to arise due to transitions from the $^6H_{15/2}$ ground state to the higher energy excited states. The frequencies of these transitions in KBS glass as well as those in ZBLANP fluoride glass [11], GeO_2-based GTK glass [2], phosphate-based PKAMF (mol % $56P_2O_5$-$17K_2O$-$18Al_2O_3$-15MgO-$4AlF_3$) [64], lead-borate ZPB ($45.0ZnO–15PbO–40B_2O_3$) [65] glasses and aqueous solution [56] are listed in Table 2 to correlate band position with covalent character. It must also be mentioned here that in the chalcogenide glass having stoichiometric composition of 0.7 $GeSe_2$–$0.2AsSe_{3/2}$–$0.1GaSe_{3/2}$ and ~ 93 % covalent character, the $^6H_{15/2} \rightarrow {}^6F_{7/2}$ and $^6H_{15/2} \rightarrow {}^6H_{7/2}$, $^6F_{9/2}$ absorption bands are red-shifted to 920 and 1110 nm respectively [54]. The $^6H_{15/2} \rightarrow {}^4I_{15/2}$ transition generally has very weak intensity due to its magnetic dipole character while all the other observed transitions have electric dipole nature. The transitions from the next excited state $^6H_{13/2}$ due to thermalization may be ruled out as the energy gap between $^6H_{15/2}$ and $^6H_{13/2}$ is quite large (~ 3000 cm^{-1}) [8].

Emission spectrum of 0.7 wt% Dy_2O_3 doped KBS antimony glass excited at 387 nm is shown in Fig. 5(b). Four emission bands are observed to be centered at 487 (blue, strong), 527 (green, weak), 579 (yellow, very strong) and 668 (red, very weak) nm are attributed to $^4F_{9/2} \rightarrow {}^6H_{15/2}$, $^4I_{15/2} \rightarrow {}^6H_{13/2}$, $^4F_{9/2} \rightarrow {}^6H_{13/2}$ ($^4G_{11/2} \rightarrow {}^6H_{11/2}$) and $^4F_{9/2} \rightarrow {}^6H_{11/2}$ respectively. These bands are compared with the bands obtained in other hosts such as ZBLANP fluoride [11], fluoro-borate BBD (mol % $79B_2O_3$-$20BaF_2$-$1Dy_2O_3$) [39], borate LBLB (mol % $8Li_2O$-7BaO-$15La_2O_3$-$70B_2O_3$) [5] and GTK glasses [2] (Table 3). The position, intensity and color of certain transitions of rare-earth ions are found to be strongly influenced by the surrounding host environment around the ion. Such electronic

transitions, termed as hypersensitive transitions, are known to obey the selection rule $\Delta J \leq 2$, $\Delta L \leq 2$ and $\Delta S \leq 0$ [8]. For the Dy^{3+} ion in KBS glass the $^4F_{9/2} \rightarrow {}^6H_{13/2}$ transition is found to be hypersensitive [8]. Here the ratio of integrated intensity of the red: yellow: green: blue emission is 1 : 32 : 2 : 18. The mixing of two primary colors, red and green, results in blue light. Consequently, the overall ratio of the blue: yellow light becomes about 2 : 3 and thereby leading to emission of intense white light. The green emission is rarely observed in other oxide hosts. But in this KBS glass it is observed that its intensity is almost twice that of the red emission. This indicates multi-channel transitions of Dy^{3+} in KBS antimony glass due to its low phonon energy and site asymmetry of Dy^{3+}.

Under 387 nm excitation, the Dy^{3+} ions are excited to ($^4F_{7/2}$, $^4I_{13/2}$) levels from which multiphonon relaxation takes place mainly resulting in the population of the $^4F_{9/2}$ level and probably the $^4I_{15/2}$ and $^4G_{11/2}$ levels to some extent due to the low phonon energy of the glass. Multi-phonon relaxation from the $^4F_{9/2}$ level to the next lower level $^6F_{3/2}$ does not take place because of large energy difference (7935 cm^{-1}) between the two levels because a minimum of thirteen photons (calculated $p = 13$) are required for bridging the $^4F_{9/2} \rightarrow {}^6F_{3/2}$ multiphonon relaxation process. Thus the population of the metastable $^4F_{9/2}$ level is highly increased leading to high rates of radiative blue and yellow transitions in contrast to those in high phonon energy glasses. Similarly, in this antimony glass host, the population of the metastable $^4G_{11/2}$ level is also increased because multiphonon relaxation processes from $^4G_{11/2}$ to the next lower $^4I_{15/2}$ level requires three bridging phonon. The high phonon orders (phonons ≥ 3) due to the low phonon energy of the glass host which decreases the possibility of non-radiative multiphonon bridging and consequently manifests the multi-channel emission processes.

The $^4I_{15/2}$ level is populated from the $^4F_{9/2}$ via thermal equilibrium because of the small energy difference (~919 cm^{-1}) between them. The transitions occur very fast in upward and downward directions between $^4F_{9/2}$ and $^4I_{15/2}$ levels. The probability of transitions from $^4F_{9/2}$ to $^4I_{15/2}$ levels at temperature T follows the Boltzmann distribution law and can be expressed as:

$$N_I/ N_F (\%) = \exp (-\Delta E_g/ k_B T) \times 100, \quad (5)$$

Where N_I and N_F are the number of Dy^{3+} ions in the $^4I_{15/2}$ and $^4F_{9/2}$ levels respectively, thus N_I/ N_F represents their relative population, k_B is the Boltzmann constant, and ΔE_g (= 919 cm^{-1}). At room temperature, k_BT = 201.6 cm^{-1} [35] hence N_I/ N_F (%) ≈ 1.5 % which is very small. For this reason, the fluorescence intensity at 527 nm is much lower.

Generally color is represented by the color coordinates of the chromaticity diagram. The chromaticity coordinates have been calculated from the emission spectra by the method using the 1931 CIE (Commission International de l'Eclairage France) system. The CIE tristimulus values expressed as integrals (or sums) are calculated for D6500 illuminant values [66]. As shown in Fig. 5(c), the color coordinates of the Dy^{3+}-doped KBS glass is calculated to be (0.35, 0.38). This color coordinate exactly fall within the white region of the CIE diagram and is very close to the standard white light color coordinates (0.33, 0.33) demarcated as ideal white in Fig. 5(c). The tendency of the color coordinates of Dy^{3+} doped KBS glass towards yellow region indicates that the intensity of yellow component is higher than that of the blue component, which is also revealed in Fig. 5(b).

3.6 Holmium, Ho^{3+} ($4f^{10}$)

Figure 6(a) along with its inset shows distinctly resolved absorption peaks of the Ho^{3+}-ions in KBS glass with assigned transitions arising from the $^5I_8$ ground state [3,15,56]. The exact positions of the absorption bands are listed in Table 2. The absorption band positions are compared with ZBLANP fluoride [11], oxyfluoro-phosphate BACSM (mol % $7Ba(PO_3)_2$-$32AlF_3$-$30CaF_2$-$18SrF_2$-$13MgF_2$) [15], SANZ (mol % $45SiO_2$-$10Al_2O_3$-$15Na_2O$-$30ZnF_2$-$0.5Ho_2O_3$) [67], TZBLH (mol % $70TeO_2$–15ZnO–10Bi2O3–$4La_2O_3$–$1Ho_2O$) glasses [26] and aqueous solution [56] to associate absorption band positions with covalent character of the host. It is worth noting that chalcogenide glass (mol %) $60GaS_{3/2}$-$10GeS_2$-$30LaS_{3/2}$ with 87% covalent character exhibits the $^5I_8 \rightarrow {}^5F_5$, $^5I_8 \rightarrow$ ($^5S_2$, $^5F_4$) and $^5I_8 \rightarrow {}^3F_3$ absorption bands at 653, 545 and 490 nm respectively [68]. The $^5I_8 \rightarrow {}^5G_6$ absorption band shows high intensity. It has happened due to its hypersensitive pseudoquadrupole transition character with large value of the reduced matrix element, $\langle U^{(2)} \rangle^2 = 1.5201$ and it obeys the selection rules $|\Delta J| \leq 2$; $|\Delta L| \leq 2$; $\Delta S = 0$ [3,8]. Hence it must be very sensitive to the glass composition and also to the Ho^{3+} ion concentration. The weak $^6H_{15/2} \rightarrow {}^4I_{15/2}$ transition has a magnetic dipole nature [3,8] while other transitions are electric dipole ones.

Figure 6(b) presents the emission spectrum of Ho^{3+}-doped glass with a 453 nm excitation wavelength. Three emission bands at 495 nm, 549 nm and 664 nm are observed from this spectrum, which could be ascribed to the $^5F_3 \rightarrow {}^5I_8$, ($^5S_2$, $^5F_4$) $\rightarrow {}^5I_8$ and $^5F_5 \rightarrow {}^5I_8$ transitions respectively. The emission wavelengths are compared with those obtained in ZBLANP fluoride [11], oxyfluoro-phosphate BACSM [15], germanium based GBZL (mol % $50GeO_2$–$20B_2O_3$–10ZnO–20LiF) [69], and phosphate BAPH (mol

% $36BaO\text{-}2Al_2O_3\text{-}60P_2O_5\text{-}1Ho_2O_3$) [70] glasses to corelate emission band positions with covalent character of the host.

The excitation of Ho^{3+} ions by 453 nm radiation initially results in the population of the $^5G_5$ level from which non-radiative multiphonon relaxation takes place to the $^5F_3$ and $^5F_4$ levels through the $^5F_1$, $^5G_6$, $^3K_8$ and $^5F_2$ levels. The number of photons required to bridge non-radiatively by $^5F_3 \rightsquigarrow {}^5F_4$ (~1998 cm^{-1}) and $^5F_4 \rightsquigarrow {}^5S_2$ (~ 3060 cm^{-1}) multiphonon relaxation is three and five respectively. Thus, although the population of the $^5F_3$ and ($^5S_2$, $^5F_4$) is increased leading to high rate of blue and green radiative transitions, but the probability of population enrichment of the $^5F_5$ level by multiphonon relaxation is sufficiently decreased due to the high photon order. The population in the metastable $^5F_5$ level in such low phonon materials occurs mainly by cross-relaxation process between Ho^{3+} ions in the ground state and $^5F_3$ level as: ($^5I_8$, $^5F_3$) → ($^5I_7$, $^5F_5$). This results in comparatively weak red $^5F_5 \rightarrow {}^5I_8$ emission. It is to be noted that similar emission spectrum is also recorded in low phonon oxyfluoro-phosphate glass (where $\hbar\omega$ = 621 cm^{-1}) [15].

3.7 Thulium, Tm^{3+} ($4f^{12}$)

Figure 7(a) shows the absorption spectrum of the Tm^{3+}-doped KBS antimony glass in the range 380-1100 nm. All transitions in the absorption spectrum of Tm^{3+} start from the ground state $^3H_6$ to the various excited states. The spectrum is characterized by four absorption bands centered at 466.5, 660.0, 688.7 and 793.3 nm corresponding to the transitions arising from the $^3H_6$ ground state to the different higher levels $^1G_4$, $^3F_2$, $^3F_3$, and $^3F_4$ (Table 2) [56]. The absorption bands measured are all dominated by electric-

dipole transitions. In Table 2 these band positions are compared with those observed in ZBLANP fluoride [11], oxyfluoride germanate GBZLL (mol % $50GeO_2$–$10B_2O_3$–$10ZnO$–10- Li_2O–$20LaF_3$) [41], zinc-boro-silicate (mol % $60ZnO$-$20B_2O_3$-$19.8SiO_2$-$0.2Tm_2O_3$) [71], zinc-antimony-borate ZSB (mol % $20ZnO$-$40Sb_2O_3$-$39B_2O_3$-$1Tm_2O_3$) [31] glasses and aqueous solution [56]. The emission spectrum of the Tm^{3+}-doped KBS glass with 466 nm is shown in Fig. 7(b) which shows an emission band located at 654 nm. In high phonon glasses, this band has been attributed to the combined effect of the $^1G_4 \rightarrow {}^3F_4$ and $^3F_2 \rightarrow {}^3H_6$ transitions. However, due to the low phonon energy of our KBS glass, we believe that this broad emission band with FWHM about 15 nm possibly arises mainly due to $^1G_4 \rightarrow {}^3F_4$ electronic transition [2]. In Table 4 the emission wavelengths of Tm^{3+} ions are compared with ZBLANP fluoride [11], GeO_2-based GNK (mol % $50GeO_2$–$25Nb_2O_5$–$25K_2O$ (Ref. [58]), GeO_2-based GTK [2] and calcium-antimony-borate CSB (mol % $20CaO$–$40Sb_2O_3$–$39B_2O_3$-$1Tm_2O_3$) [31] glasses.

Under excitation at 466 nm, the Tm^{3+} ions are excited to $^1G_4$ level from which mainly radiative transitions takes place to the $^3F_4$ level. Multiphonon relaxation from $^1G_4$ to $^3F_2$ level is less likely to take place due to the low phonon energy of the KBS host. To bridge the $^2G_4 \rightarrow {}^3F_2$ energy gap (~6250 cm^{-1}), a minimum of ten (calculated p = 10) photons is required which is considerably high. Consequently, population of the metastable $^1G_4$ level is increased leading to high intensity red $^1G_4 \rightarrow {}^3F_4$ emission.

3.8 Neodymium, Nd^{3+} ($4f^3$); Samarium, Sm^{3+} ($4f^5$); Erbium, Er^{3+} ($4f^{11}$); Ytterbium, Yb^{3+} ($4f^{13}$)

In our previous papers we performed a detailed spectroscopic analysis of KBS antimony glasses doped with Nd^{3+}, Sm^{3+} and Er^{3+} ions. Like the ZBLANP glass [11], Nd^{3+} ions in KBS did not exhibit any down-shifting however upconversion was observed [36]. The Sm^{3+} and Er^{3+} ions displayed both downshifting and upconversionin kBs antimony glass [34,35]. The Sm^{3+} ion exhibited more intense deep-red $^4G_{5/2} \rightarrow {}^6H_{9/2}$ electric dipole transition than the orange $^4G_{5/2} \rightarrow {}^6H_{7/2}$ magnetic dipole or green $^4G_{5/2} \rightarrow {}^6H_{5/2}$ emission due to low-phonon energy of KBS glass and additional electric field induced by highly polarizable chemical environment (Sb^{3+} ion has very high polarizability due to its large size and lone pair of electrons) possessing a low symmetry geometric configuration [34]. The calculated molar polarizability (from Lorentz–Lorenz equation) of KBS antimony glass is found to be 9.598 $Å^3$ which is considerably greater than the molar polarizability of silica glass (2.965 $Å^3$). The Er^{3+} ions exhibited green ($^2H_{11/2} \rightarrow {}^4I_{15/2}$ and $^4S_{3/2} \rightarrow {}^4I_{15/2}$) as more intense red emission ($^4F_{9/2} \rightarrow {}^4I_{15/2}$) again due to low phonon energy of KBS glass [35]. In Table 3, the emission bands of the Sm^{3+} and Er^{3+} ions in KBS glass have been compared with the band positions obtained in ZBLANP [11] other glass hosts [25,42,65,49,72]. The Yb^{3+} ion shows an absorbance band centered at 977.4 nm (Fig. 8) due to $^2F_{7/2} \rightarrow {}^2F_{5/2}$ transition [73] but due to inadequate instrumental facility we could not perform the photoluminescence of Yb^{3+} ion in KBS antimony glass. A comparison of the full-width-half-mean (FWHM) values of the main emission bands of various RE^{3+} ions in KBS glass with other glasses [74-86] is given in Table 4.

3.9 Lanthanum, La^{3+} ($4f^0$); Cerium, Ce^{3+} ($4f^1$); Promethium, Pm^{3+} ($4f^4$); Gadolinium, Gd^{3+} ($4f^7$); Lutecium, Lu^{3+}($4f^{14}$)

We could not characterize the behavior of the Ce^{3+}, Pm^{3+}, Gd^{3+} and Lu^{3+} ions in high Sb_2O_3 containing KBS glasses due to several limitations. The Ce^{3+} ion is known to exhibit absorption band in the UV region (around 245 nm) and exhibits broad emission between 380-480 nm [8]. Since the UV cut off wavelength or absorption edges of high antimony glass is about 370 nm, the high absorption of the host glass hinders the exploitation of the Ce^{3+} ion. Although Pm^{3+} is expected to exhibit some weak bands between 400-476 nm, however Pm^{3+} ion is radioactive and undergoes decomposition to daughter products. Gd^{3+} represents a half-filled shell of equivalent electrons, but it can display absorption bands all of which lies in the UV region of the spectrum from 193-312 nm. The La^{3+} and Lu^{3+} ions do not reveal any $f \rightarrow f$ transitions due to vacant and fully-filled *f*-shells respectively.

3.10 Quantitative justification of UV-Vis-NIR absorption and emission band position

Earlier in 1985, Reisfeld had tabulated the wavelengths of the NIR emission transition of Nd^{3+} ion is various glasses and it clearly showed that the emission wavelengths red-shifts from fluoride to oxide to chalcogenide [55]. Dominiak-Dzik et al [27] have observed a red-shifting of the absorption bands of Pr^{3+} towards higher wavelengths with the decrease in PbF_2 content in lead-based oxyfluoride glass. Some authors have attributed such shifting to covalency of the host [17], however this have not yet been clearly ascertained with explicit generalized studies. Consequently, one of the primary objectives of this systematic study is to establish that the covalent character of the glass host, which originates due to nephelauxetic effect, plays the critical role in determining the positions of both the absorption and emission bands despite the fact that

the 4f electrons of the RE^{3+} ions are considerably shielded by 5s and 5p electrons. From the examination of the UV-Vis-NIR absorption positions and visible emissions of the RE^{3+} ions in various hosts in Table 2 and 3, it is obvious that the bands position shifts towards higher wavelength with the increase in calculated covalent character of the host. This shift can be interpreted in terms of chemical bonding property of the ligand (here oxygen, halogen, chalcogen or chalcohalogen) due to the so-called "nephelauxetic effect" (literally means "charge cloud expansion"). The well known "spectrochemical series" is also another important consequence of "nephelauxetic effect".

The concept of "nephelauxetic effect" was introduced by Jørgensen [87]. The effect occurs for transition metal as well as for RE^{3+} ions. The "nephelauxetic effect" provides an indirect but convincing evidence of metal-ligand orbital overlap. It occurs due to metal-ligand bond formation, that is, overlap between the metal and ligand orbitals forming larger molecular orbital leading to delocalization of the electron cloud over a larger area. According to Jørgensen [87], owing to this effect, the phenomenological parameters of interelectron repulsion are smaller in a host than in the corresponding free ions. The separation between various Russell-Saunders states depend on certain inter-electronic repulsion parameters called "Racah parameters" which is found to have nearly 70 % lower value in complexes (here glass host) than the corresponding free ions [88]. Such decrease in interelectron repulsion suggests a wider separation between the same orbital-electrons, as if the electron clouds have "expanded" to some extent. As the covalency of the metal–ligand bond increases, the ligands transfer some charge to the metal or RE^{3+} ion. Thus, the ligands will reduce the effective positive charge on the metal and allow for some expansion of the *f*-shell. This nephelauxetic effect decreases the

interelectronic repulsion parameters of valence electrons of an ion in the crystal/glass host in comparison with their free-ion value due to covalency of bonds between the central ion and ligands. Thus covalent bonding may have the effect of lowering the electronic levels of the free ion due to the nephelauxetic effect. This exerts influences on the position of the absorption bands and thereby influence on the emission bands is also noticed. Here, it may be noted that the nephelauxetic shift is largely more discernible for those transitions in which the electric dipole-dipole type interaction dominates.

Mathematically, the total Hamiltonian for an individual RE^{3+} ion in a crystal field (or ligand field), H_{CF} (matrix) is the sum of the free ion (H_{FI}) and the interaction potentials due to crystal field within the host [87].

$$H_{CF} = H_{core} + H_{e\text{-}e} + H_{spin\text{-}orbit} + H_{static\ lattice} + H_{dynamic\ lattice} \quad (6)$$

where $H_{FI} = H_{core} + H_{e\text{-}e} + H_{spin\text{-}orbit}$. The H_{core} describes the movement of the independent electrons in the coulomb field of the central core. $H_{e\text{-}e}$ and $H_{spin\text{-}orbit}$ are inter-electronic repulsion and spin-orbital coupling parameter respectively. $H_{static\ lattice}$ arises due to the static crystal field (assuming the ligands to be point charges). The coulomb field of the surrounding ions (ligands) lowers the symmetry of the Hamilton operator leading to splitting of energy levels. $H_{dynamic\ lattice}$ arises due to vibronic interaction. The importance of these perturbations lies in the ability to cause an admixing of states of opposite parity, breaking of certain symmetry, therein permitting radiative dipole transitions between various levels. For a RE^{3+} ion ion solid host, the order of perturbations is [87]:

$$(H_{core} + H_{e\text{-}e}) > H_{spin\text{-}orbit} >> H_{static\ lattice} > H_{dynamic\ lattice} \quad (7)$$

Other perturbations are much smaller and may be neglected. So, when an ion is incorporated into a host, due to nephelauxetic effect, the parameters H_{core}, $H_{e\text{-}e}$ and $H_{spin\text{-}}$

$_{orbit}$ are reduced from their free ion values. All these causes a contraction of the energy level structure of the ion in that particular host compared to that of free ion. Consequently the wavelength of absorption and thereby also the emission bands are shifted towards lower value. The main factors known to affect the nephelauxetic effect are covalency and polarizabilities of bonds, overlap of wave functions, coordination number for host, valence states of ions and also possibly some other elements, like, changes of anisotropy of bonds.

There are many theoretical approaches for describing the effect quantitatively. From the absorption spectra of RE^{3+} ions in the glasses, the nephelauxetic effect or shift in energy level position (β) can be calculated using the following relations: [87]

$$\beta = \Sigma\, n\beta^*/n \qquad (8)$$

where $\beta^* = \nu_c/\nu_a$. The ν_c and ν_a are energies of the corresponding transitions in investigated complex/glass host and free-ion/aqua ion [56,61,62], respectively, and n denotes the number of levels used for β values calculation. The calculated values of β for the RE^{3+} ions in KBS, fluoride (ZBLANP) and other glass hosts is also given in Table 2.

The covalency or degree of covalent bonding character of a host can be estimated approximately using the formula:

$$\text{Covalent character (\%)} = \exp\,[-0.25\,(\Delta\chi)^2] \times 100 \qquad (9)$$

where $\Delta\chi$ is the electronegativity of the glass, that is, the electronegativity difference (χ_A-χ_C) of the anions and the cations. The average electronegativity of anions (χ_A) or cations (χ_C) can be evaluated by the following simple additive relation [15]:

$$\chi_A \text{ or } \chi_C = \Sigma\, N_i\, \chi_i \,/\, \Sigma\, N_i \qquad (10)$$

where N_i and χ_i are the number of individual constituent atom per mole and its electronegativity (in Pauling's scale) respectively.

The lower value of the nephelauxetic parameter β indicates more covalency in the RE-ligand bond. This is in agreement with the relationship between β and bonding parameter (δ) proposed by Sinha [89]:

$$\delta = [(1-\beta)/\beta] \times 100 \qquad (11)$$

Positive or negative sign of δ indicates covalent or ionic bonding of the RE-ligand bond.

From Table 2, it is observed that in KBS glass the covalent contributions to the Pr^{3+}–ligand (here O^{2-}) and Eu^{3+}–O^{2-} are greater than that of Tb^{3+}–O^{2-}, Dy^{3+}–O^{2-} and Ho^{3+}–O^{2-} bonds. This can be explained as an influence on post Gd elements due to the phenomenon of lanthanide contraction which results in decrease in ionic radii of the elements in the lanthanide series. In 8-coordinated oxide system the ionic radius of Pr^{3+}, Eu^{3+}, Tb^{3+}, Dy^{3+} and Ho^{3+} ions are 1.14, 1.07, 1.04, 1.03 and 1.02 Å [90]. The smaller sizes of Tb^{3+}, Dy^{3+} and Ho^{3+} ions make them less polarizable. It can also be observed from Table 2 that the values β generally increase with decrease in covalent character of the host.

The nephelauxetic effect is explained by Jørgensen as an expansion of the partly filled shell ($4f^{n-1}$ of RE ions) due to the transfer of the ligands to the core of the central RE^{3+} ion. The F^- ion due to its high electronegativity, small size, high charge density and very small polarization forms ionic bonds. The polarizability of the O^{2-} anion by cations of the glass systems is greater than that of the F^- ion due to its comparatively larger size, greater charge and lesser electronegativity. Consequently, metal-oxygen (M-O) bond has considerable covalent property with directional property. Such covalent character are

introduced by overlap of p-orbital of O^{2-} ion with the f-orbital of RE^{3+} or d-orbital of Sb^{3+} with the formation of larger molecular orbitals and thereby leading to an expansion of the electron clouds, decrease in inter-electron repulsions or enhanced nephelauxetic effect. Thus, the covalent character of the glass increases. The extent to which the O^{2-} anion is polarized by various cations is governed by Fajan's Rules of polarization depending upon the ionic potential, electronegativity and electronic configuration of the respective cations [87]. With the increase covalent character, that is, the overlap of the ligands and metal orbitals, the energy level structure of the RE^{3+} ion contracts and this leads to a shift of absorption bands towards the smaller energies. Therefore, an obvious and reliable correlation exists between the nephelauxetic parameter and the covalent bonding characteristics of various hosts of the RE^{3+} ion. Besides, Tables 2 and 3 give possible indications that the absorption and emission properties can be tuned by controlling the covalency of the host.

Table 4 suggests the possibility that the FWHM of RE^{3+} emissions decreases in the order conventional oxide glasses < HMO glasses < fluoride glasses. Earlier Reisfeld [55] had indicated a similar correlation of FWHM of Nd^{3+} ion with phonon energy of glasses but it is difficult to affirm any conclusion because the broadening (inhomogeneous) of luminescence spectra of RE^{3+} in various glasses depends on a variety of factors like RE^{3+} environment, vibration of the surrounding ligands, presence of different phonon modes, random RE^{3+} cation distribution, temperature , scattering effects, relaxation process, dielectric-network structure, and other local parameters.

3.11 Judd-Ofelt (J-O) Theory and Calculation of the J-O Spectroscopic Parameters

The Judd-Ofelt (J-O) theory is the most well accepted method generally used by physicist for spectroscopic investigation of RE^{3+} ions in various environments (transparent medium). Using the J-O theory, three phenomenological spectroscopic parameters Ω_2, Ω_4 and Ω_6 are experimentally evaluated considering the from the experimental absorption spectra and refractive index of the host material and the theoretical values of the three matrix elements $U^{(2)}$, $U^{(4)}$ and $U^{(6)}$, connecting any pair of electronic levels of the $4f^n$ configuration [91]. These Ω_λ parameters, are be used to predict a lot of useful information regarding efficiency and performance of the luminescent material.

Generally the hypersensitive (pseudoquadrupolar) transitions have very large values of $U^{(2)}$ and it was found that the intensity of the hypersensitive transition of any RE^{3+} ion generally increases with the increase of covalency between the RE^{3+} ion and the surrounding ligand environment. Since, in the determination of the J-O parameters, the area of the hypersensitive absorption band is considered, so the chemists put forward a more simple correlation that Ω_2 parameter is related to the covalency of the metal–ligand bond and can be used to monitor the covalency changes in glasses [91]. So in case of a RE^{3+} ion incorporated in a glassy matrix (oxide, halide or chalcogenide), the amount of covalency existing in the RE-ligand (O, F, Cl, Br, I, S, Se, etc) bonds can be inferred from the intensity and nature of hypersensitive transitions. The Ω_2 is also suggested to depend on distortions in the crystal field of the rare-earth ion from cubic symmetry. The parameters Ω_4 and Ω_6 are to a large extent independent of Ω_2. They are related to the rigidity of the host medium in which the ions are situated [92].

The relevant modus operandi of the J-O model has been well described elsewhere [25]. Here we provide a short synopsis to analyze the J-O parameters of Nd^{3+}, Ho^{3+}, and Er^{3+} ions in KBS antimony oxide glass because these ions have a large number of absorption bands in the visible region which minimizes the calculation errors to a large extent [93].

According to the Judd–Ofelt (J-O) theory, the experimentally measured electric and magnetic dipole line strength of an electronic transition from an initial $(S,L)J$ state to the final $(S',L')J'$ state are given by:

$$S_{ed}^{meas}\ (J \rightarrow J') = \frac{3ch\,(2J+1)\,n}{8\pi^3\lambda_{max}e^2N}\left[\frac{9}{(n^2+2)^2}\right]\frac{2.303}{d}\int_{(J\rightarrow J')} OD(\lambda)d\lambda - nS_{md}^{meas} \qquad (12)$$

where $S_{ed}^{meas}(J\rightarrow J')$ and S_{md}^{meas} is the measured electric dipole and magnetic dipole line strength, λ_{max} is the mean wavelength of the absorption band, 'n' is the refractive index of the host, 'd' is the thickness of the sample under study, 'N' is the concentration of RE^{3+} ions (ions/cm^3) in the host, 'e' is the electronic charge, $\int_{(J\rightarrow J')} OD(\lambda)d\lambda$ represents the experimental integrated optical density in the wavelength range of the band and can be obtained by calculating the total area under the absorption band. To calculate the integrated absorption of the bands, base glass corrected absorption spectrum was used after necessary correction for the overall rise in the base line. The factor $9/(n^2 + 2)^2$ represents the local field correction for the ion is dielectric medium.

The measured magnetic dipole line strength (S_{md}^{meas}) of a transition is related to the magnetic dipole oscillator strength (F_{md}) by the equation:

$$F_{md} = [8\pi^2mc/3h(2J + 1)\,\lambda_{max}]\,S_{md}^{meas} \qquad (13)$$

where ‘m’ is the mass of the electron and ‘c’ is the velocity of light. The F_{md} values of different transitions of a series of RE^{3+} ions have also been calculated by Carnall et al. [94].

The procedure involves fitting the measured electric dipole line strengths with theoretical electric dipole line strengths $S_{ed}^{theo}(J \rightarrow J')$ which is given by the equation:

$$S_{ed}^{theo}(J \rightarrow J') = \sum \Omega_{t\,(=2,4,6)} | < (S,L)J || U^t || (S',L')J' > |^2 \qquad (14)$$

where $< (S,L)J || U^t || (S',L')J' > |$ is the reduced matrix element of the irreducible tensor operator of rank ‘t’ calculated in the intermediate coupling approximation for the transitions are almost invariant with respect to crystal field strength and depends only on the concerned RE^{3+} ion. The values of the square of the reduced matrix elements for various transitions of the RE^{3+} ions are obtained from literature [56,60,61]. Least square fitting analysis of the equations yields values of the J-O parameters corresponding to individual ions.

Consequently, the three J-O parameters of the Nd^{3+}, Ho^{3+}, and Er^{3+} ions in KBS antimony glasses have been calculated (as these ions have large number of absorption bands in the visible region minimizes the error) and compared with other different glass environments [93-108] in Table 5, 6 and 7 respectively. The variation of the parameter versus covalent character of the host has been plotted for each of these ions (Figs. 9, 10 and 11). Although the points are scattered to some extent, since large errors are often associated in the determination of J-O parameters by different authors as it depends on the transitions and fitting procedure chosen, nevertheless an obvious increase of Ω_2 values with increase of covalent character is observed.

Earlier a similar correlation has been demonstrated by Reisfeld [55,92] for several RE^{3+} ions where oxides and chalcogenide glass hosts presented a greater value of the Ω_2 intensity parameter than fluoride glasses and crystals. The Ω_2 parameters are smallest for crystals because they exhibited least covalent bonding with the rare earths. In fluoride glasses the number of different sites in which the RE^{3+} ion can be situated is much less and the symmetry of these sites is much more. Moreover they exhibit much less covalent bonding than oxide glasses. So the Ω_2 parameters obtained with fluoride glass host are smaller than that obtained with oxide glass hosts. This is exemplified by the fact that absorption and emission spectra are narrower in fluoride glasses than in oxide ones. The Ω_2 parameters were very high for the chalcogenide glasses due to their highest covalency among the glasses [55].

For glasses, the RE^{3+} ions are distributed over a large number of nonequivalent sites, more than that present in crystals, and the intensity parameters are the average values of Ω_2. In fact it has often been emphasized that symmetry alone cannot account for the enormous variation sometimes observed in the intensities of the hypersensitive transitions for different chemical environments. Theoretical calculations have shown that the dynamic coupling contribution due to the polarization of the surrounding ligands or atoms must be considered to explain the large intensity variation in different hosts.

The mechanism of dynamic coupling was originally proposed by Jørgensen and Judd [109] in an attempt to explain the unusual intensity variation of certain 4f-4f transitions classified as hypersensitive transitions. The incident radiation field induces oscillating dipoles in the ligand atoms surrounding the RE^{3+} ions and as a result, an additional oscillating electric field is produced that leads to forced electric dipole

mechanism. This additional oscillating electric field produced near the RE^{3+} ion has large local gradients and may induce 4f-4f transitions with oscillator strengths in the order of or sometimes greater than 10^6.

Thus Ω_2 is strongly enhanced by covalent bonding and this is equivalent to the dynamic polarization of the ligands by dynamic coupling and quadrupole moment of the transitions. Practically the dynamic coupling mechanism cannot be disregarded under any circumstances. When the J-O parameters Ω_λ are conventionally estimated from experimental intensities (absorption bands), the forced electric dipole and dynamic couplings are absorbed simultaneously and cannot be discriminated. This can be clearly understood by considering the Ω_2 values of $ErCl_3(AlCl_3)_x$, $ErBr_3$ and ErI_3 vapors which are 25.8×10^{-20}, 60×10^{-20} and 100×10^{-20} cm^2 respectively [55,92]. In going from the gaseous compounds of ErI_3 to $ErBr_3$ to $ErCl_3(AlCl_3)_x$, there is a drastic decrease in polarizability from the I^- ion to Br^- ion to Cl^- ion. This results in a decrease in magnitude of the intensities dominated by $\Omega_2\, U^{(2)}$, that is, the hypersensitive transitions. Generally anomalous changes of the intensities dominated by $\Omega_4\, U^{(4)}$ and $\Omega_6\, U^{(6)}$ does not occur, since for these cases the dramatic increase in the Er-X (X = Cl, Br and I) may compensate for the increase in polarizability values. This can explain the fact that nearly all glass materials containing trivalent RE^{3+} ions (and also the aqua ions and other complexes in solution) show a moderate variation of both Ω_4 and Ω_6 parameters. On contrary, the changes in the Ω_2 values which may widely varies from less than 1 to 40×10^{-20} cm^2 in condensed mater and even upto 275×10^{-20} cm^2 for NdI_3 vapor [55,92].

Thus, a correlation is noticed in the sense that glasses which exhibit a higher degree of covalency (percent covalent character) tend to present higher values of Ω_2,

suggesting that in these cases the dynamic coupling mechanism dominates. As already mentioned, the Ω_λ intensity parameters in vitreous materials correspond to statistical average values over all sites and these values determined experimentally incorporate both the forced electric dipole and the dynamic coupling contributions. The dependence of the polarizabilities of the neighboring ions confers to the latter mechanism a stronger dependence on the nature of the chemical environment. Just for comparison, considering a 100% ionic model of the ligand field interaction, the charge of both the fluorine and chlorine ions is -1, in units of the electronic charge, while their dipolar isotropic polarizabilities are, 1^3 and 3 $Å^3$ respectively. This may account for the hypersensitive behavior of certain 4f-4f transitions which are generally dominated by Ω_2 $U^{(2)}$.

4. Conclusions

The main achievement in this work is that novel rare-earth ions doped high antimony oxide containing (70 mol%) glasses in the K_2O-B_2O_3-Sb_2O_3 (KBS) system has been fabricated for the first time by melt-quench technique in ambient atmosphere. This particular glass not only has low phonon energy (602 cm^{-1}) close to that of fluoride glasses, but also has similar photoluminescence properties in the visible region when doped with different RE^{3+} ions. Evidence for low phonon energy (602 cm^{-1}) of this glass has been demonstrated by infrared reflection spectroscopy. Inspection of the UV-Vis-NIR absorption and visible emission band positions of the RE^{3+} ions in various hosts clearly exhibit a shift in position and the sequence is analogous to the shift in covalent character of the embedding host. It is unanimously and unambiguously established that the band positions shift towards higher wavelength with increase in covalent character of

the host in the order fluoride < oxyfluoride < oxide < chalcohalide (halide = Cl, Br, I) < chalcogenide. Along with the evaluation of the Judd-Ofelt parameters of Nd^{3+}, Ho^{3+}, and Er^{3+} ions in KBS antimony glass, it is also established that Ω_2 value increases with the increase in covalent character of the host in the same order. So both RE absorption and emission band positions and Ω_2 parameter (a parameter generally used by physicists) are controlled by the covalent character (a fundamental property generally used by the chemists) of the host and this influence is popularly known as "nephelauxetic effect". The calculation and generalization provide evidence for the sensitivity of this parameter to their bonding characteristics. We believe that this article would help to gain antimony glasses wider attention as potential low phonon hosts for rare-earth elements for the development of various visible solid state lasers, modern lighting and optical displays. It reinforces that spectroscopy of the RE^{3+} ions in the solid state is largely controlled by the nephelauxetic effect along with the basic insight. This study also generalizes that fine tuning of laser emissions could be achieved by controlling the covalent character of the host.

Acknowledgements

TS expresses her sincere gratitude to the financial support of the Council of Scientific and Industrial Research (CSIR), New Delhi in the form of NET-SRF under sanction number 31/015(0060)/2007-EMR-1. The authors gratefully thank Director of the institute for his kind permission to publish this paper.

References

[1] E. Sintzer, Phys.Rev. Lett. 7 (1961) 444-447.

[2] G. Lakshminarayana, J. Qiu, M. G. Brik, I. V. Kityk, J. Phys.: Condens. Matter 20 (2008) 335106 (11pp).

[3] P. Nachimuthu, R. Jagannathan, J Am. Ceram. Soc., 82 (1999) 387-392.

[4] H. Lin, E. Y. -B. Pun, X. Wang, X. Liu, J. Alloys Comp. 390 (2005) 197–201.

[5] B. Klimesz, G. Dominiak-Dzik, P. Solarz, M. Żelechower, W. Ryba-Romanowski, J. Alloys. Compd. 403 (2005) 76-85.

[6] V. V. R. K. Kumar, A. K. Bhatnagar, R. Jagannathan, J. Phys. D.: Appl. Phys. 34 (2001) 1563-1568.

[7] Y. Nageno, H. Takebe, K. Morinaga, J. Am. Ceram. Soc. 76 (1993) 3081-3086.

[8] K. Pátek, Glass Lasers, J. G. Edwards (Ed.), Butterworth, England, 1970.

[9] S. Tanabe, S. Ohyagi, N. Soga, T. Hanada, Phys. Rev. B 46 (1992) 3305-3310.

[10] J. Lucas, Curr. Opin. Solid State Mater. Sci. 2 (1997) 405-411.

[11] P. W. France, in: P. W. France, M. G. Drexhage, J. M.Parker. M. W. Moore, S. F. Carter, J. V. Wright (Eds.), Fluoride Glass Optical Fibers, Blackie, Glasgow, 1990.

[12] R. Reisfeld, G. Katz, N. Spector, C. K. Jørgensen, C. Jacoboni, R. DePape, J. Solid State Chem. 41 (1982) 253-261.

[13] S. Nishibu, S. Yonezawa, M. Takashima, J. Non-Cryst. Solids 351 (2005) 1239–1245.

[14] A. Flórez, E.M. Ulloa, R. Cabanzo, J. Alloys Comp. 488 (2009) 606–611.

[15] B. Karmakar, J. Solid State Chem. 178 (2005) 2663–2672.

[16] T. Iqbal, M. R. Shahriari, P. Hajcak, G. H. Sigel, Jr., L. R. Copeland, W. A. Reed, Appl. Opt. 33 (1994) 965-968.

[17] P. Nachimuthu, M. Vithal, R. Jagannathan, J. Am. Ceram. Soc. 83 (2000) 597–604.

[18] W.A. Pisarski, J. Pisarska, G. Dominiak-Dzik, M. Mączkac, W. Ryba-Romanowski, J. Phys. Chem. Solids 67 (2006) 2452–2457.

[19] H. Lin, G. Meredith, S. Jiang, X. Peng, T. Luo, N. Peyghambarian, E. Y. -B. Pun, J. Appl. Phys. 93 (2003) 186-191.

[20] T. F. Xu, X. Shen, Q. H. Nie, Y. Gao, Opt. Mater. 28 (2006) 241–245.

[21] X. Shen, Q. H. N., T. Feng Xu, Y. Gao, Spectrochim. Acta A 61 (2005) 2827–2831.

[22] H. Lin, S. Tanabe, L. Lin, Y. Y. Hou, K. Lin, D. L. Yang, T. C. Ma, J. Y. Yu, E. Y. B. Pun, J. Lumin. 124 (2007) 167-172.

[23] H. Lin, Y.Y. Zhang, E.Y.B. Pun, Spectrochim. Acta A 71 (2008) 1547–1550.

[24] Q. Nie L. Lu, T. Xu, S. Dai, X. Shen, X. Liang, X. Zhang, X. Zhang, J. Phys. Chem. Solids 68 (2007) 477–481.

[25] A. Ghosh, R. Debnath, Opt. Mater. 31 (2009) 604-608.

[26] G. Gao, G.Wang, C. Yu, J. Zhang, L. Hua, J. Lumin. 129 (2009) 1042–1047.

[27] G. Dominiak-Dzik, W. Ryba-Romanowski, J. Pisarska, W. A. Pisarski, J. Lumin. 122-123 (2007) 62-65.

[28] W. A. Pisarski, J. Mol. Struct. 744–747 (2005) 473–479.

[29] G. J. Quaries, A. Suchockki, R. C. Powell, J. Appl. Phys. 63 (1988) 861-870.

[30] W. Vogel, Glass Chemistry, Springer-verlag, Berlin, 1992

[31] T. Som, B. Karmakar, J. Non-Cryst. Solids 356 (2010) 987–999.

[32] K. S. V. Sudhakar, T. Satyanarayana, L. Srinivasa Rao, M. Srinivasa Reddy, N. Veeraiah, Solid State Commun. 146 (2008) 441–445.

[33] Q. Qian, Y. Wang, Q.Y. Zhang, G.F. Yang, Z.M. Yang, Z.H. Jiang, J. Non-Cryst. Solids 354 (2008) 1981–1985.

[34] T. Som, B. Karmakar, J. Lumin. 128 (2008) 1989-1996.

[35] T. Som, B. Karmakar, Opt. Mater. 31 (2009) 609-618.

[36] T. Som, B. Karmakar, J. Alloy Comp. 476 (2009) 383-389.

[37] P. J. Miller and C. A. Cody, Spectrochim. Acta A 38 (1982) 555-559.

[38] H. Lin, S. Tanabe, L. Lin, D. L. Yang, K. Liu, W. H. Wong, J. Y. Yu, E. Y. B. Pun, Phys. Lett. A 358 (2006) 474-477.

[39] Y. Dwivedi, S. B. Rai, Opt. Mater. 31 (2009) 1472-1477.

[40] X. Liang, C. Zhu, Y. Yang, S. Yuan, G. Chen, J. Lumin.128 (2008) 1162–1164.

[41] G. Lakshminarayana, H. Yang, J. Qiu, J. Solid State Chem. 182 (2009) 669-676.

[42] G. Lakshminarayana, R. Yang, J. R. Qiu, M. G. Brik, G. A. Kumar, I. V. Kityk, J. Phys. D: Appl. Phys. 42 (2009) 015414 (12 pp.).

[43] R. V. Deun, K. Binnemans, C. Görller-Walrand, J. L. Adam, J. Alloys Comp. 283 (1999) 59–65.

[44] T. T. Murata, H. Takebe, K. Morinaga, J. Am. Ceram. Soc. 81 (1998) 249-251.

[45] B. Karmakar, R. N. Dwivedi, J. Non-Crystalline Solids 342 (2004) 132-139.

[46] S. Todoroki, S. Tanabe, K. Hirao, N. Soga**,** J. Non-Cryst. Solids 136 (1991) 213-218.

[47] R. Cases and M. A. Chamarro, J. Solid State Chem. 90 (1991) 313-319.

[48] S. Xu, G. Wang, J. Zhang, S. Dai, L. Hu, Z. Jiang, J. Non-Cryst. Solids 336 (2004) 230–233.

[49] S. Xu, G. Wang, J. Zhang, S. Dai, J. Zhang, L. Hu, Z. Jiang, J. Lumin. 109 (2004) 187-192.

[50] Y. S. Han, J. H. Song, J. Heo, J. Am. Ceram. Soc. 87 (2004) 1381–1383.

[51] Z. Shang, G. Ren, Q. Yang, C. Xu, Y. Liu, Y. Zhang, Q. Wu, J. Alloys Comp. 460 (2008) 539–543.

[52] S. J. L. Ribeiro, J. Dexpert-Ghys, B. Piriou, V. R. Mastelaro, J. Non-Cryst. Solids 159 (1993) 213-221.

[53] R. Reisfield, Spectroscopy of rare-earth ions, in Nanostructured and Advanced Materials, A. Vaseashta, D. Dimova-Malinovska, J. M. Marshall (Eds.), Springer, 2005, pp. 77-100.

[54] R. Jing, Y. Guang, Z. Huidan, Z. Xianghua, Y. Yunxia, C. Guorong, J. Am. Ceram. Soc., 89 (2006) 2486–2491.

[55] R. Reisfeld, Journal of the Less-Common Metals, 112 (1985) 9– 18.

[56] W. T. Carnall, P. R. Fields, K. Rajnak, J. Chem. Phys. 49 (1968) 4424-4442.

[57] R. Balda, J. Fernández, A. De Pablos, J. M. Fdez-Navrro, J. Phys.: Condens. Mater. 11 (1999) 7411-7421.

[58] G. Lakshminarayana, J. Qiu, M. G. Brik, I. V. Kityk, J. Phys. D: Appl. Phys. 41 (2008) 175106 (10pp).

[59] T. Miyakawa, D. L. Dexter, Phys. Rev. B 1 (1970) 2961-2969.

[60] A. Kumar, D.K. Rai, S.B. Rai, Spectrochim. Acta A 58 (2002) 2115–2125.

[61] W. T. Carnall, P. R. Fields, K. Rajnak, J. Chem. Phys. 49 (1968) 4450-4455.

[62] W. T. Carnall, P. R. Fields, and K. Rajnak, J. Chem. Phys. 49 (1968) 4447-4449.

[63] S. Rai, S. Hazarika, Opt. Mater. 30 (2008) 1343–1348.

[64] Ch. Basavapoornima, C. K. Jayashankar, P. P. Chandrachoodan, Physica B 404 (2009) 235-242.

[65] A. Thulasiramudu, S. Buddhudu, Spectrochim. Acta Part A 67 (2007) 802–807.

[66] Bamford C R. Colour Generation and Control in Glass. Amsderdam: Elsevier; 1977.

[67] L. Feng, J. Wang, Q. Tang, L. Liang, H. Liang, Q. Su, J. Lumin. 124 (2007) 187–194.

[68] K. Kadono, M. Shojiya, M. Takahashi, H. Higuchi, Y. Kawamoto, J. Non-Cryst. Solids 259 (1999) 39-44.

[69] G. Lakshminarayana, J. Qiu, M. G. Brik, G. A. Kumar, I. V. Kityk, J. Phys.: Condens. Matter 20 (2008) 375104 (12pp).

[70] T. Satyanarayana, T. Kalpana, V. Ravi Kumar, N. Veeraiah, J. Lumin. 130 (2010) 498–506.

[71] K. Annapurna, Maumita Das, S. Buddhudu, Physica B 388 (2007) 174–179.

[72] G. Lakshminarayana, S. Buddhudu, Physica B 373 (2006) 100–106.

[73] L.R.P. Kassab, M.E. Fukumoto, V.D.D. Cacho, N.U. Wetter, N.I. Morimoto, Opt. Mater. 27 (2005) 1576–1582.

[74] C.H. Kam, S. Buddhudu, J. Quant. Spectros. Rad. Tran. 85 (2004) 1–12.

[75] H. Lin, D. Yang, G. Liu, T. Ma, B. Zhai, Q. An, J. Yua, X. Wang, X. Liu, E. Y. B. Pun, J. Lumin. 113 (2005) 121–128.

[76] G. Tripathi, V. K. Rai, S.B. Rai, Optics Commun. 264 (2006) 116–122.

[77] S. Balaji, P. Abdul Azeem, R.R. Reddy, Physica B 394 (2007) 62–68.

[78] C.H. Kam, S. Buddhudu, Physica B 337 (2003) 237–244.

[79] V. K. Rai, S.B. Rai, D.K. Rai, Optics Commun. 257 (2006) 112–119.

[80] C.H. Kam, S. Buddhudu, Solid State Commun. 128 (2003) 309–313.

[81] M. Seshadri, Y. C. Ratnakaram, D. T. Naidu, K. V. Rao, Opt. Mater. 32 (2010) 535–542.

[82] A. K. Singh, S.B. Rai, V.B. Singh, J. Alloys Compd. 403 (2005) 97–103.

[83] C.H. Kam, S. Buddhudu, Microelectronics Journal 34 (2003) 849–854.

[84] L. Srinivasa Rao, M. Srinivasa Reddy, M.V. Ramana Reddy, N. Veeraiah, Physica B 403 (2008) 2542–2556.

[85] Y. K. Sharma, S. S. L. Surana, R. K. Singh, R. P. Dubedi, Opt. Mater. 29 (2007) 598–604.

[86] B. Sudhakar Reddy, S. Buddhudu, K. S. R. K. Rao, P. Naresh Babu, K. Annapurna, Spectros. Lett. 41 (2008) 376–384.

[87] C. K. Jørgensen, Modern Aspects of Ligand Field Theory, North-Holland, Amsterdam, 1971.

[88] G. Racah, Phys. Rev. 62 (1942) 438-462.

[89] S.P. Sinha, Complexes of the Rare Earth, Pergamon Press, Oxford, 1966.

[90] A. A. Kaminskii, Laser Crystals, Their Physics and Properties, 2nd edition, Springer-Verlag, Berlin, Heidelberg, 1990.

[91] B. G. Wybourne, Spectroscopic Properties of Rare Earths, Interscience, New York, 1975.

[92] C. K Jørgensen, R. Reisfeld, J. Less-Common Metals 93 (1983) 107-112.

[93] K Binnemans, C Görller-Walrand, J. Phys.: Condens. Matter 10 (1998) L167–L170.

[94] W.T. Carnall, P.R. Fields, K. Rajnak, J. Chem. Phys. 49 (1968) 4412.

[95] G. Lakshminarayana, M. Mao, R. Yang, J. R.Qiu, M.G. Brik, Physica B 404 (2009) 3348–3355.

[96] R.T. Karunakaran, K. Marimuthu, S. Arumugam, S. S. Babu, S. F. Leon-Luis, C.K. Jayasankar, Opt. Mater. 32 (2010) 1035-1041.

[97] M. Seshadri, K. Venkata Rao, J. Lakshmana Rao, K.S.R. Koteswara Rao, Y. C. Ratnakaram, J. Lumin. 130 (2010) 536–543.

[98] G.N. Hemantha Kumar, J.L. Rao, K. Ravindra Prasad, Y.C. Ratnakaram, J. Alloys Comp. 480 (2009) 208–215.

[99] L.S. Griscom, J.-L. Adam, K. Binnemans, J. Non-Cryst. Solids 256 & 257 (1999) 383-389.

[100] L.X. Yi, M. Wang, S.Y. Feng, Y.K. Chen, G.N. Wang, L.L. Hu, J.J. Zhang, Opt. Mater. 31 (2009) 1586–1590.

[101] Y.C. Ratnakaram, N.V. Srihari, D. T. Naidu, A. Vijayakumar, R.P.S. Chakradhar, Opt. Mater. 30 (2008) 1635–1643.

[102] M. Seshadri, Y.C. Ratnakaram, D. T. Naidu, K. V. Rao, Opt. Mater. 32 (2010) 535–542.

[103] N. V. V. Prasad, K. Annapurna, N. S. Hussain, S. Buddhudu, Mater. Lett. 57 (2003) 2071-2080.

[104] D. Chen, Y. Wang, Y. Yu, E. Ma, J. Solid State Chem.179 (2006) 1445–1452.

[105] Y. Luo, J. Zhang, J. Sun, S. Lu, X. Wang, Opt. Mater. 28 (2006) 255–258.

[106] G.A. Kumar, E. De la Rosa, H. Desirena Opt. Commun. 260 (2006) 601–606.

[107] S. Dai, J. Wu, J. Zhang, G. Wang, Z. Jiang, Spectrochim. Acta A 62 (2005) 431–437.

[108] H. Lin, K. Liu, E.Y.B. Pun, T.C. Ma, X. Peng, Q.D. An, J.Y. Yu, S.B. Jiang, Chem. Phys. Lett. 398 (2004) 146–150.

[109] C. K. Jørgensen, B. R. Judd, Mol. Phys. 8 (1964) 281-290.

Table 1
Comparison of the phonon energy of KBS antimony oxide glass with other glass hosts.

Glasses/ Glass composition (mol %)	Average/ exact phonon energy (cm^{-1})	Reference
Borate	~ 1400 (1340-1480)	[53,55]
Phosphate	~ 1200 (1200-1350)	[53,55]
Silicate	~ 1100 (1060-1150)	[53,55]
Germanate	~ 900 (800-975)	[53,55]
$90GeO_2$-$10Na_2O$	850	[44]
$80GeO_2$-$20Na_2O$	805	[44]
$70GeO_2$-$30Na_2O$	770	[44]
Lead		
73.5 PbO–$18.5B_2O_3$–$5Al_2O_3$–$3WO_3$	1300	[27]
70PbO–$30B_2O_3$	1250	[52]
20PbO–$60GeO_2$	~ 820	[51]
56PbO-$44GeO_2$	~ 790	[51]
72.5PbO-26.0SiO_2-1K_2O-0.5Na_2O (wt%)	990	[45]
Gallate		
$40Ga_2O_3$-$30K_2O$-$30Ta_2O_5$	730	[44]
60Ga2O3-$30K_2O$-10Ta_2O5	713	[44]
Tellurite	~ 700	[53]
$75TeO_2$-$7.5Li_2O$-$7.5K_2O$-5BaO-$5Bi_2O_3$	746	[23]
$50TeO_2$–50PbO	737	[52]
$70TeO_2$-30LiF	690	[6]
$80TeO_2$-20BaO	610	[44]
Bismuth-gallate		
$50Bi_2O_3$-$30Ga_2O_3$-$5Li_2O$-$5K_2O$-10BaO	673	[23]
Lead-bismuth-gallate		
57PbO–$25Bi_2O_3$–$18Ga_2O_3$	~ 550	[50]
Antimony oxide		
$15K_2O$-$15B_2O_3$-$70Sb_2O_3$ (KBS)	602	This study
Fluorides/ Heavy metal fluorides	~ 500-600	
$45InF_3$-$14ZnF_2$-$19BaF_2$-$17SrF_2$-$3GaF_3$-$2LaF_3$	500	[27]
51.5ZrF_4-19.5BaF_2-5.3LaF_3-3.2AlF_3-18NaF-2.5PbF_2 (ZBLANP)	~ 500	[11]
52ZrF_4-18BaF_2-3LaF_3-2AlF_3-25CsBr	~ 490	[47]
Oxyfluoro-phosphate		
7$Ba(PO_3)_2$-32AlF_3-30CaF_2-18SrF_2-13MgF_2	621	[15]
Heavy metal oxyfluorides		
$20B_2O_3$–$80PbF_2$	1100	[52]
$50SiO_2$-$50PbF_2$	904	[49]
$53GeO_2$–$47PbF_2$	783	[52]
$50TeO_2$–$50PbF_2$	745	[52]
Chalcogenides	~ 300-450	[53,54,55]

Table 2
Comparison of UV-Vis-NIR absorption bands and their associated transitions of various RE^{3+} ion doped KBS antimony glass with other glasses and aqueous solution

RE^{3+} ion / transitions	Hosts/ Absorption band position (nm)					
Pr^{3+} ion						
	KBS antimony glass	ZBLANP glass [11]	IZBSGL glass [27]	Aqueous solution [56]	PTO glass [17]	PGO glass [57]
$^3H_4 \rightarrow {}^1D_2$	593.5	587	591.9	593.8	595.2	593.0
$^3H_4 \rightarrow {}^3P_0$	485.3	478	484.7	481.9	481.9	4850
$^3H_4 \rightarrow {}^3P_1$	472.3	466	472.0	469.5	472.8	473.0
$^3H_4 \rightarrow {}^3P_2$	445.7		445.8	444.0	446.0	446.0
C_{cov} (%)	46.5	14	20	61	63.5	68
β	0.996	1.0091	0.9970		0.9966	0.9957
Eu^{3+} ion						
	KBS antimony glass	ZBLANP glass [11]	TL glass [60]	Aqueous solution [61]	BPAWE glass [18]	
$^7F_1 \rightarrow {}^5D_1$	533.5		533	534.9	533.8	
$^7F_0 \rightarrow {}^5D_1$	525.8	524	525	525.5	526.5	
$^7F_0 \rightarrow {}^5D_2$	464.5	464	463.0	464.7	464.8	
$^7F_1 \rightarrow {}^5D_3$	412.0		414	409.7		
$^7F_0 \rightarrow {}^5L_6$	393.6	393	391.0	393.7	394	
C_{cov} (%)	46.5	14	48	61	68	
β	0.9995	1.0021	1.0009		0.9998	
Tb^{3+} ion						
	KBS antimony glass	ZBLANP glass [11]		Aq. Soln. [62]		
$^7F_6 \rightarrow {}^5D_4$	485.8	485		486.7		
C_{cov} (%)	46.5	14		61		
β	1.0019	1.0036				
Dy^{3+} ion						
	KBS antimony glass	ZBLANP glass [11]	GTK glass [2]	PKAMF glass [64]	ZPB glass [65]	Aqueous solution [56]
$^6H_{15/2} \rightarrow {}^6F_{9/2}, {}^6H_{7/2}$	1078.9	-	1082	1095.0	1096.0	1098.9
$^6H_{15/2} \rightarrow {}^6H_{5/2}$	975.7	973		-		980.4
$^6H_{15/2} \rightarrow {}^6F_{7/2}$	894.9	906	893	901.1	906.0	909.1
$^6H_{15/2} \rightarrow {}^6F_{5/2}$	803.8	804	795	804.0	805.0	806.4
$^6H_{15/2} \rightarrow {}^6F_{3/2}$	750.5	752	746	754.0	755.0	754.7
$^6H_{15/2} \rightarrow {}^4I_{15/2}$	452.8	-	454	453.0	-	452.5
C_{cov} (%)	46.5	14	40	49	57	61
β	1.0079	1.0044	1.01128	1.0189	1.0018	-

Ho^{3+} ion						
	KBS antimony glass	ZBLANP glass [11]	BACSM glass [15]	SANZ glass [67]	TZBLH glass [26]	Aqueous solution [56]
$^5I_8 \rightarrow {}^5F_5$	643.0	639	640.5	641.0	645	645.2
$^5I_8 \rightarrow {}^5S_2, {}^5F_4$	537.3	535	536.2	537.0	539	540.5
$^5I_8 \rightarrow {}^5F_3$	485.2	483	484.5	486.0	-	485.4
$^5I_8 \rightarrow {}^5F_2$	472.9	-	472.5	-	-	473.9
$^5I_8 \rightarrow {}^3K_8$	467.5	467	466.6	-	-	467.9
$^5I_8 \rightarrow {}^5G_6$	453.1	448	450.6	448	451	-
$^5I_8 \rightarrow {}^5F_1$	449.9	-	-	-	-	-
$^5I_8 \rightarrow {}^5G_5$	417.3	415	416.2	418	419	417.5
C_{cov} (%)	46.5	14	18	39	57	61
β	1.0019	1.0076	1.0044	1.0027	0.9998	
Tm^{3+} ion						
	KBS antimony glass	ZBLANP glass [13]	GBZLL glass [41]	ZBSi glass [71]	ZSB glass [31]	Aqueous solution [56]
$^3H_6 \rightarrow {}^3F_4$	793.3	790	792	792	795	787.4
$^3H_6 \rightarrow {}^3F_3$	688.7	683	683	686	692	689.7
$^3H_6 \rightarrow {}^3F_2$	666.0	658	-	662	664	662.2
$^3H_6 \rightarrow {}^1G_4$	466.5	463	466	467	468	468.2
C_{cov} (%)	46.5	14	44	52	59	61
Yb^{3+} ion						
	KBS antimony glass	ZBLANP glass [13]	PBG Glass [73]			
$^2F_{7/2} \rightarrow {}^2F_{5/2}$	977.4	974	978			
C_{cov} (%)	46.5	14	64			

Host compositions (mol %):
Aqueous solution = 100 H_2O
BACSM = $7Ba(PO_3)_2$-$32AlF_3$-$30CaF_2$-$18SrF_2$-$13MgF_2$ (Ref. [15])
BPAWE = $10B_2O_3$-$80PbO$-$6Al_2O_3$-$3WO_3$-$1Eu_2O_3$ (Ref. [18])
GBZLL = $50GeO_2$–$10B_2O_3$–10ZnO–10- Li_2O–$20LaF_3$ (Ref. [41])
GTK glass = $60GeO_2$–$20TiO_2$–$20K_2O$ (Ref. [2])
IZBSGL = 45InF3–14ZnF2–19BaF2–17SrF2–3GaF3–2LaF3 (Ref. [28])
KBS = $15K_2O$-$15B_2O_3$-$70Sb_2O_3$ [This study]
PBG = $56.46PbO$–$31.17Bi_2O_3$–$12.37Ga_2O_3$ (Ref. [73])
PGO = 60PbO-40GeO2 (Ref. [57])
PKAMF = $56P_2O_5$-$17K_2O$-$18Al_2O_3$-15MgO-$4AlF_3$ (Ref. [64])
PTO = $70PbO$-$30TiO_2$ (Ref. [17])
SANZ = $45SiO_2$-$10Al_2O_3$-$15Na_2O$-$30ZnF_2$-$0.5Ho_2O_3$ (Ref. [67]
TL = $80TeO_2$-$20Li_2CO_3$ (Ref. [56])
TZBLH = $70TeO_2$–15ZnO–$10Bi_2O_3$–$4La_2O_3$–$1Ho_2O_3$ (Ref. [26])
ZBSi = $60ZnO$-$20B_2O_3$-$19.8SiO_2$-$0.2Tm_2O_3$ (Ref. [71])
ZBLANP = $51.5ZrF_4$-$19.5BaF_2$-$5.3LaF_3$-$3.2AlF_3$-18NaF-$2.5PbF_2$ (Ref. [11])
ZPB glass = 45.0ZnO–15PbO–$40B_2O_3$ (Ref. [65])
ZSB = $20ZnO$-$40Sb_2O_3$-$39B_2O_3$-$1Tm_2O_3$ (Ref. [31])
C_{cov} (%) = percent covalent character and β = Nephelauxetic parameter.

Table 3
Comparison of main visible emission bands of various RE^{3+} ions and their associated transitions in KBS antimony glass with other hosts

RE^{3+} ion / transitions	Hosts/ Emission band position (nm)				
Pr^{3+} ion					
	KBS antimony glass	ZBLANP glass [11]	IZBSGL Glass [27]	GNK glass [58]	PTO glass [17]
$^3P_0 \rightarrow {}^3H_6$	607	603	603	616	617
$^3P_0 \rightarrow {}^3F_2$	652	635	636	648	647
C_{cov} (%)	46.5	14	20	38	63.5
Eu^{3+} ion					
	KBS antimony glass	ZBLANP glass [11]	GTK glass [2]	TL glass [60]	
$^5D_0 \rightarrow {}^7F_1$	595	591	592	592.2	
$^5D_0 \rightarrow {}^7F_2$	617	615	614	613.6	
$^5D_0 \rightarrow {}^7F_4$	705	698	702	701.0	
C_{cov} (%)	46.5	14	40	48	
Tb^{3+} ion					
	KBS antimony glass	ZBLANP glass [11]	SALG glass [42]	GTK glass [2]	PAKB glass [63]
	547	543	545	549	-
	587	585	587	586	590
	626	621	622	621	625
C_{cov} (%)	46.5	14	38	40	50
Dy^{3+} ion					
	KBS antimony glass	ZBLANP glass [11]	BBD glass [39]	GTK glass [2]	LBLB glass [4]
$^4F_{9/2} \rightarrow {}^6H_{15/2}$	487		481	485	486 nm
$^4F_{9/2} \rightarrow {}^6H_{13/2}$	579	575	573	576	579 nm
$^4F_{9/2} \rightarrow {}^6H_{11/1}$	668	661	663	665	-
C_{cov} (%)	46.5	14	21	40	50
Ho^{3+} ion					
	KBS antimony glass	ZBLANP glass[11]	BACSM glass[15]	GBZL glass [69]	BAPH glass [70]
$^5F_3 \rightarrow {}^5I_8$	495		491	-	494
$^5S_2, {}^5F_4 \rightarrow {}^5I_8$	549	543	543	555	555
$^5F_5 \rightarrow {}^5I_8$	664		658	658	659
C_{cov} (%)	46.5	14	18	49	54

Tm^{3+} ion					
	KBS antimony glass	ZBLANP glass[11]	GNK glass [58]	GTK glass [2]	CSB glass [31]
$^1G_4 \rightarrow {}^3F_4$	654	649	650	650	659
C_{cov} (%)	46.5	14	38	40	59

Sm^{3+} ion					
	KBS antimony glass [33]	ZBLANP glass[11]	SALG glass [42]	ZPB glass [65]	BZP glass [72]
$^4G_{5/2} \rightarrow {}^6H_{5/2}$	566	560	563	563	564
$^4G_{5/2} \rightarrow {}^6H_{7/2}$	602	595	599	598	602
$^4G_{5/2} \rightarrow {}^6H_{9/2}$	652	641	645	646	647
$^4G_{5/2} \rightarrow {}^6H_{11/2}$	702		706	708	710
C_{cov} (%)	46.5	14	38	57	63

Er^{3+} ion					
	KBS antimony glass [34]	ZBLANP glass[11]	TBBL glass [25]	SOPF glass [49]	POPF glass [3]
$^4S_{3/2} \rightarrow {}^4I_{15/2}$	549	543	542	543	550
$^4F_{3/2} \rightarrow {}^4I_{15/2}$	658	655	650	655	677
$^2H_{11/2} \rightarrow {}^4I_{15/2}$	528		519	525	532
C_{cov} (%)	46.5	14	45	53	55

Host glass compositions (mol %):

BAPH= $36BaO\text{-}2Al_2O_3\text{-}60P_2O_5\text{-}1Ho_2O_3$ (Ref. [70])
BBD glass = $79B_2O_3\text{-}20BaF_2\text{-}1Dy_2O_3$ (Ref. [37])
BZP = $45B_2O_3\text{-}5ZnO\text{-}50PbO$ (Ref. [72])
CSB = $20CaO–40Sb_2O_3–39B_2O_3\text{-}1Tm_2O_3$ (Ref. [31])
GBZL = $50GeO_2–20B_2O_3–10ZnO–20LiF$ (Ref. [69])
GNK = $50GeO_2–25Nb_2O_5–25K_2O$ (Ref. [58])
LBLB = $8Li_2O\text{-}7BaO\text{-}15La_2O_3\text{-}70B_2O_3$ (Ref. [5])
PAKB = $60P_2O_5\text{-}10Al_2O_3\text{-}20K_2O\text{-}10BaO$ (Ref. [63])
POPF = $30PbO\text{-}70PbF_2$ (Ref. [3])
SALG = $50SiO_2–20Al_2O_3–10Li_2O–20GdF_3$ (Ref. [42])
SOPF = $50SiO_2\text{-}50PbF_2$ (Ref. [49]).
TBBL = $80TeO_2\text{-}15BaF_2\text{-}15BaO\text{-}4La_2O_3\text{-}1Er_2O_3$ (Ref. [25])
ZPB = $45.0ZnO–15PbO–40B_2O_3$ (Ref. [65])
C_{cov} (%) = percent covalent character
For composition of ZBLANP, IZBSGL, PTO, GTK, TL, and BACSM glasses refer to footnote of Table 2.

Table 4
Comparison of full-width-half-mean (FWHM) of the main visible emission bands of various RE^{3+} ions in KBS antimony glass with other glass hosts.

RE^{3+} ion/ Emission transitions	Full width at half mean (FWHM) (nm) of RE^{3+} ions in various host glasses				
Pr^{3+} ion					
	PTO [17]	PTEO [17]	ZBLYAN [74]	GNK [58]	KBS
$^3P_0 \rightarrow {}^3H_6$	38	33	30 ± 2	28	27
Eu^{3+} ion					
	LBaLaB [75]	BLC [76]	GTK [2]	NBA [77]	KBS
$^5D_0 \rightarrow {}^7F_1$		9.6	11	11.2	13
$^5D_0 \rightarrow {}^7F_2$	15	10.9	12	11.7	11
Tb^{3+} ion					
		ZBLYAN [78]	GTK [2]	PAKB [63]	KBS
$^5D_4 \rightarrow {}^7F_5$		17	14	17	11
$^5D_4 \rightarrow {}^7F_4$		16	17	21	16
$^5D_4 \rightarrow {}^7F_3$		15	15	23	12
Dy^{3+} ion					
	TL [79]	ZBLYAN [80]	GTK [2]	GNK [58]	KBS
$^4F_{9/2} \rightarrow {}^6H_{15/2}$	15.1	18.5	17		15
$^4F_{9/2} \rightarrow {}^6H_{13/2}$	13.2	19.4	16	15	14
Ho^{3+} ion					
		PNC [81]	LKBBG [23]	TL [82]	KBS
$^5S_2, {}^5F_4 \rightarrow {}^5I_8$		29	17	14.38	17
$^5F_5 \rightarrow {}^5I_8$		52	24	13.12	
Tm^{3+} ion					
		ZrZnABY [83]	GTK [2]	GNB [58]	KBS
$^1G_4 \rightarrow {}^3F_4$		11	7	7	11

Sm^{3+} ion	LBLB [75]	LNBSm [84]	LMBSm [84]	LWBSm [84]	KBS
$^4G_{5/2} \rightarrow {}^6H_{5/2}$		14	17	18	11
$^4G_{5/2} \rightarrow {}^6H_{7/2}$	17	16	20	21	17
$^4G_{5/2} \rightarrow {}^6H_{9/2}$		25	26	28	13

Er^{3+} ion	SNCKBAs [85]	BPZL [86]	BPCL [86]	BPTL [86]	KBS glass
$^4S_{3/2} \rightarrow {}^4I_{15/2}$	22.5	20.5	18.1	19.8	16
$^4F_{3/2} \rightarrow {}^4I_{15/2}$					
$^2H_{11/2} \rightarrow {}^4I_{15/2}$	10.5	-	-	-	10

Host glass compositions (mol %):

BLC = $69B_2O_3$-$20Li_2O$-$10CaO$-$1Eu_2O_3$ (Ref. [76]

BPCL = 69.8 B_2O_3–10 P_2O_5–10CdO–10 LiF (Ref. [86])

BPTL = 69.8 B_2O_3–10 P_2O_5–10TeO_2–10 LiF (Ref. [86])

BPZL = 69.8 B_2O_3–10 P_2O_5–10ZnO–10 LiF (Ref. [86])

LBaLaB = $8Li_2O$- 7BaO-$14La_2O_3$-$70B_2O_3$-1Eu2O3 (Ref. [75])

LKBBG = Li_2O–K_2O–BaO–Bi_2O_3–Ga_2O_3 (Ref: [23])

LMB = 40 Li_2O–4 MoO_3–55 B_2O_3-1.0 Ln_2O_3 (Ref: [84])

LNB = 40 Li_2O–4 Nb_2O_5–55 B_2O_3-1.0 Ln_2O_3 (Ref. [84])

LWB = 40 Li_2O–4 WO_3–55 B_2O_3-1.0 Ln_2O_3 (Ref. [84])

NBA = 8NaF- $81B_2O_3$ -$10Al_2O_3$-$1Eu_2O_3$ (Ref. [77])

PNC = $69.5P_2O_5$ -$15Na_2O$-15CaO-$0.5Ho_2O_3$ (Ref: [81])

PTEO = $70PbO_2$-$30TeO_2$ (Ref. [17])

SNCKBAs = (wt %) $68.94SiO_2$–$22.55Na_2O$–1.91CaO–$4.96K_2O$–$0.85B_2O_3$–$0.29As_2O_3$–$0.5Er_2O_3$ (Ref. [85])

ZBLYAN = $53ZrF_4$–$20BaF_2$–$2LaF_3$–$2YF_3$–$3AlF_3$–19 NaF glass (Refs. [74,78, 80])

ZrZnABY = $20ZrF_4$–$30ZnF_2$ –$25AlF_3$–$10BaF_2$–$15YF_3$ (Ref: [83])

For composition of PTO, GTK, TL glasses refer to footnote of Table 2 while for composition of GNK, PAKB, LBLB glasses refer to footnote of Table 3

Table 5
Variation of the Judd-Ofelt parameters ($\times 10^{-20}$) of neodymium (Nd^{3+}) ion with glass composition and covalent character

Glass composition (mol %)	Covalent character (%)	Judd-Ofelt parameter			Reference
		Ω_2	Ω_4	Ω_6	
Heavy metal fluorophosphate $35InF_3$-$20ZnF_2$-$8BaF_2$-$8P_2O_5$- $20SrF_2$-$6GaF$-$2NaF$-$1ErF_3$	26.05	1.3002	0.3761	0.8013	[14]
$30PbO$-$70PbF_2$	32.79	1.528	3.620	3.821	[3]
Fluorophosphate $75NaPO_3$–$24LiF$–$1NdF_3$	36.06	3.44	4.14	6.28	[93]
Fluorosilicate $50SiO_2$-$20Al_2O_3$-$20CaF_2$-$10GdF_3$	36.44	5.252	3.242	4.419	[95]
Fluoroborate $49.5B_2O_3$-$49.5NaF$-$1Nd_2O_3$	40.17	7.79	3.03	2.86	[96]
Antimony oxide $15K_2O$-$15B_2O_3$-$70Sb_2O_3$ (KBS)	46.50	7.87	2.21	9.37	[This study]
Phosphate $69P_2O_5$-$15Na_2O$-$15K_2O$-$1Nd_2O_3$	50.42	7.68	8.96	11.71	[97]
$69.9P_2O_5$-$15Na_2O$-$15K_2O$- $0.1Nd_2O_3$	50.86	8.03	5.73	11.31	[98]
Chalcohalide $50GeS_2$-$25Ga_2S_3$-$25CsCl$	79.17	7.09	8.99	5.03	[99]
$50GeS_2$-$25Ga_2S3$-$25CsBr$	80.12	10.8	13.1	6.79	[99]
$50GeS_2$-$25Ga_2S_3$-$25CsI$	81.52	11.3	11.3	7.58	[99]

Table 6
Variation of the Judd-Ofelt parameters ($\times 10^{-20}$) of the holmium (Ho^{3+}) ion with glass composition and covalent character

Glass composition (mol %)	Covalent character (%)	Judd-Ofelt parameter			Reference
		Ω_2	Ω_4	Ω_6	
Heavy metal oxyfluoride					
$50HoF_3$-$20BaF_2$-$10AlF_3$-$20GeO_2$	19.67	0.05	0.10	0.02	[13]
$10HoF_3$-$20BaF_2$-$10AlF_3$-$60GeO_2$	23.07	1.96	0.64	0.11	[13]
Fluorophosphate					
$20Al(PO_3)_3$-$47BaF_2$-$13MgF_2$-20LiF	31.04	3.11	3.50	1.65	[100]
Fluorosilicate					
$45SiO_2$-$10Al_2O_3$-$15Na_2O$-$30ZnF_2$-$0.5Ho_2O_3$	38.86	5.84	2.38	1.75	[67]
Antimony oxide					
$15K_2O$-$15B_2O_3$-$70Sb_2O_3$ (KBS)	46.50	3.83	1.78	2.18	[This study]
Tellurite					
$70TeO_2$-10ZnO-10ZnF2-$2.5K_2O$-$2.5Na_2O$-5LaO	47.10	4.2	2.8	1.1	[26]
Bismuth-gallate					
$5Li_2O$-$5K_2O$-10BaO-$50Bi_2O_3$-$30Ga_2O_3$	48.08	6.753	2.674	5.049	[23]
Phosphate					
$69.5P_2O_5$-$15Li_2CO_3$-$15K_2CO_3$-$0.5Ho_2O_3$	50.97	7.793	4.709	2.365	[101]
$69.5P_2O5$-$15Na_2O$-$15K_2O$-$0.5Ho_2O_3$	51.00	8.58	4.31	2.88	[102]
Boro-tellurite					
$20TeO_2$-$75B_2O3$-$5Li_2O$	55.08	7.59	7.69	4.29	[103]

Table 7
Variation of the Judd-Ofelt parameters ($\times 10^{-20}$) of erbium (Er^{3+}) ion with glass composition and covalent character

Glass composition (mol %)	Covalent character (%)	Judd-Ofelt parameter			Reference
		Ω_2	Ω_4	Ω_6	
Heavy metal fluorophosphates					
$35InF_3$-$20ZnF_2$-$8BaF_2$-$8P_2O_5$-$20SrF_2$-$6GaF$-$2NaF$-$1ErF_3$	26.05	1.3002	0.3761	0.8013	[26]
$30PbO$-$70PbF_2$	32.79	3.216	1.338	0.609	[3]
Fluorosilicate					
$50SiO_2$-$20Al_2O_3$-$20CaF_2$-$10GdF_3$	36.44	4.847	0.7719	1.2549	[95]
$44.5SiO_2$–$24.8Al_2O_3$–$5.0CaO$–$9.9NaF$–$14.8CaF_2$-$1ErF_3$	37.02	4.40	1.61	1.12	[104]
Germanate					
$10Na_2O$-$90GeO_2$	39.46	5.72	0.62	0.47	[44]
Bismuth-gallate					
$5Li_2O$-$5K2O$-$10BaO$-$50Bi_2O_3$-$30Ga_2O_3$	42.40	5.66	1.39	0.74	[22]
Fluoro-tellurite					
$80TeO_2$-$15BaF_2$-$15BaO$-$4La_2O_3$-$1Er_2O_3$	44.60	4.935	3.148	1.745	[25]
Antimony oxide					
$15K_2O$-$15B_2O3$-$70Sb_2O_3$ (KBS)	46.50	6.23	3.08	1.42	[This study]
Tellurite					
$36TeO_2$-$36WO_3$-$18Li_2O$-$10Er_2O_3$	47.88	6.58	1.72	1.20	[105]
$75TeO_2$-$14ZnO$-$10Na2O$-$1Er2O3$	51.76	5.98	1.32	1.47	[106]
$80TeO2$-$20BaO$	53.49	5.88	1.15	1.56	[44]
$20Nb_2O_5$- $80TeO_2$	56.69	6.21	1.54	1.14	[107]
$15Ga_2O_3$-$75TeO_2$	60.59	6.46	1.64	1.47	[108]
Bismuth-tellurite					
$70TeO_2$-$15WO_3$-$10Bi_2O_3$	64.76	6.57	1.25	1.10	[20]
$70TeO_2$–$20WO_3$–$10Bi_2O_3$	65.23	6.06	1.57	0.95	[21]
Borate					
$75B_2O_3$-$15K_2O$	72.67	7.31	1.70	0.87	[9]

Figure Captions

Fig. 1. Infrared reflection spectrum (IRRS) of the KBS antimony oxide base glass having composition $15K_2O–15B_2O_3–70Sb_2O_3$ (mol%).

Fig. 2. (a) Absorption and (b) emission spectrum of 0.7 wt% Pr_2O_3 doped KBS antimony oxide glass (thickness: 2 mm, a.u. is absorbance unit, λ_{ex} is excitation wavelength, c.p.s. is cycles per second).

Fig. 3. (a) Absorption and (b) emission spectrum of 0.7 wt% Eu_2O_3 doped KBS antimony oxide glass (thickness: 2 mm, a.u. is absorbance unit, λ_{ex} is excitation wavelength, c.p.s. is cycles per second).

Fig. 4. (a) Absorption and (b) emission spectrum of 0.7 wt% Tb_2O_3 doped KBS antimony oxide glass (thickness: 2 mm, a.u. is absorbance unit, λ_{ex} is excitation wavelength, c.p.s. is cycles per second).

Fig. 5. (a) Absorption and (b) emission spectrum of 0.7 wt% Dy_2O_3 doped KBS antimony glass (thickness: 2 mm, a.u. is absorbance unit, λ_{ex} is excitation wavelength, c.p.s. is cycles per second).

Fig. 5(c). Calculated CIE color coordinates for white luminescence of Dy^{3+} doped KBS antimony glass marked as solid (●).

Fig. 6. (a) Absorption and (b) emission spectrum of 0.7 wt% Ho_2O_3 doped KBS antimony oxide glass (thickness: 2 mm, a.u. is absorbance unit, λ_{ex} is excitation wavelength, c.p.s. is cycles per second).

Fig. 7. (a) Absorption and (b) emission spectrum of 0.7 wt% Tm_2O_3 doped KBS antimony glass (thickness: 2 mm, a.u. is absorbance unit, λ_{ex} is excitation wavelength, c.p.s. is cycles per second).

Fig. 8. Absorption spectrum of 0.7 wt% Yb_2O_3 doped KBS antimony glass (thickness: 2 mm, a.u. is absorbance unit).

Fig. 9. Variation of Judd-Ofelt parameter ($\Omega_2 \times 10^{-20}$) of the Nd^{3+} ion as a function of covalent character of various glasses (HMFP is heavy metal fluorophosphates, HMOF is heavy metal oxyfluoride, KBS is K_2O-B_2O_3-Sb_2O_3 glass of this study and R is correlation coefficient in case of linear fit).

Fig. 10. Variation of Judd-Ofelt parameter ($\Omega_2 \times 10^{-20}$) of the Ho^{3+} ion as a function of covalent character of various glasses (HOMF is heavy metal oxyfluoride, KBS is K_2O-B_2O_3-Sb_2O_3 glass of this study and R is correlation coefficient in case of linear fit).

Fig. 11. Variation of Judd-Ofelt parameter ($\Omega_2 \times 10^{-20}$) of the Er^{3+} ion as a function of covalent character of various glasses (HMFP is heavy metal fluorophosphates, HOMF is heavy metal oxyfluoride, KBS is K_2O-B_2O_3-Sb_2O_3 glass of this study and R is correlation coefficient in case of linear fit). The dotted area represents the probable value of Ω_2 parameter of the Er^{3+} in heavy metal oxide host.

Figures

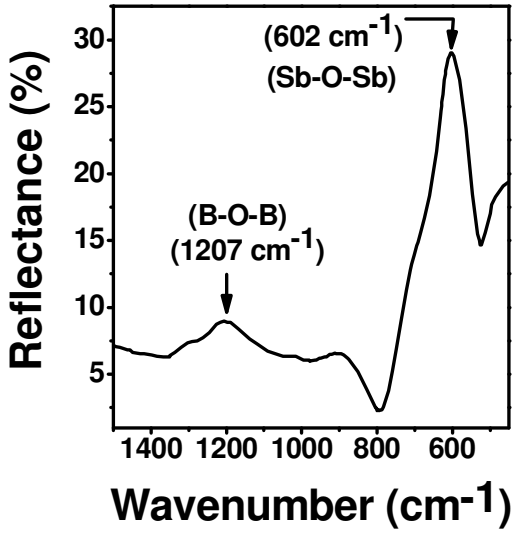

Fig. 1.

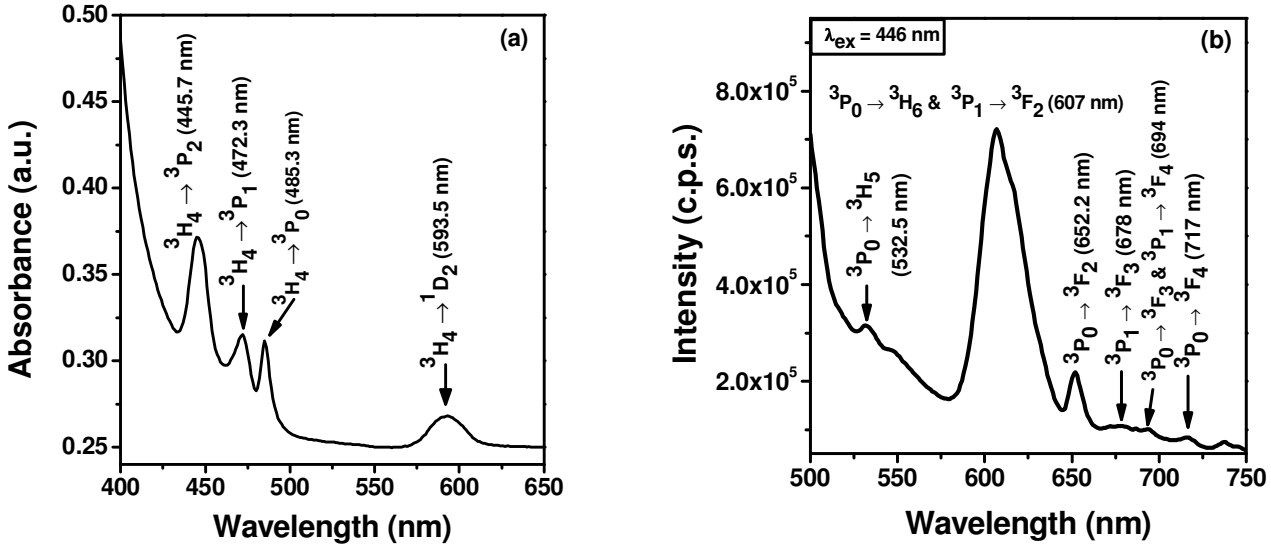

Fig. 2. (a) and (b).

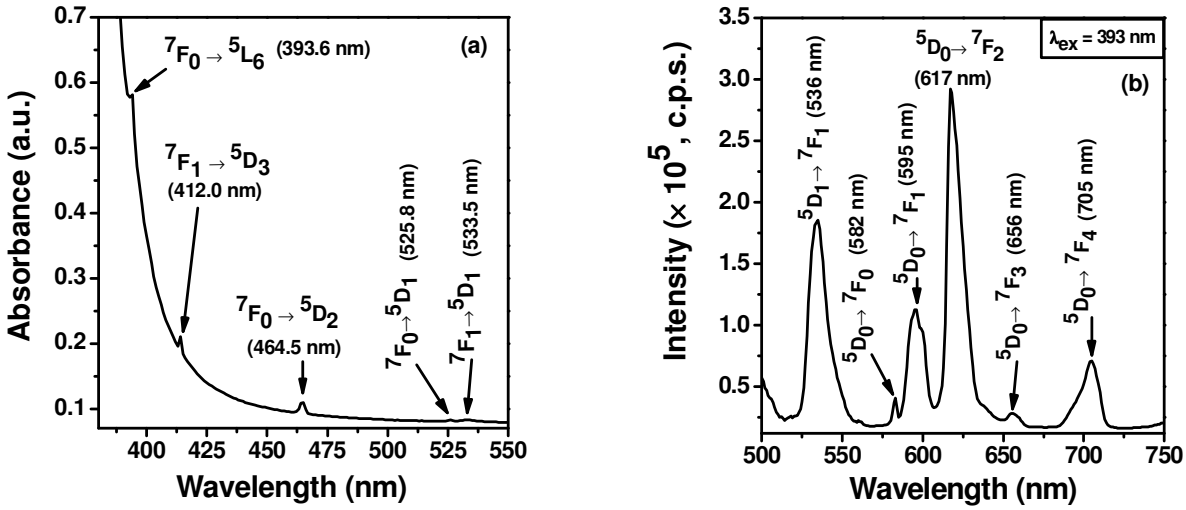

Fig. 3. (a) and (b).

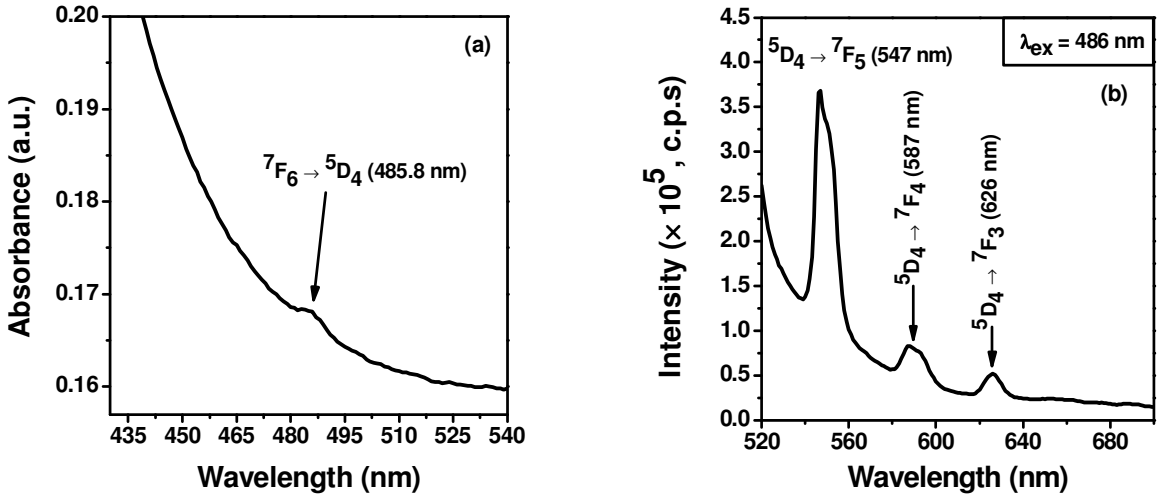

Fig. 4. (a) and (b).

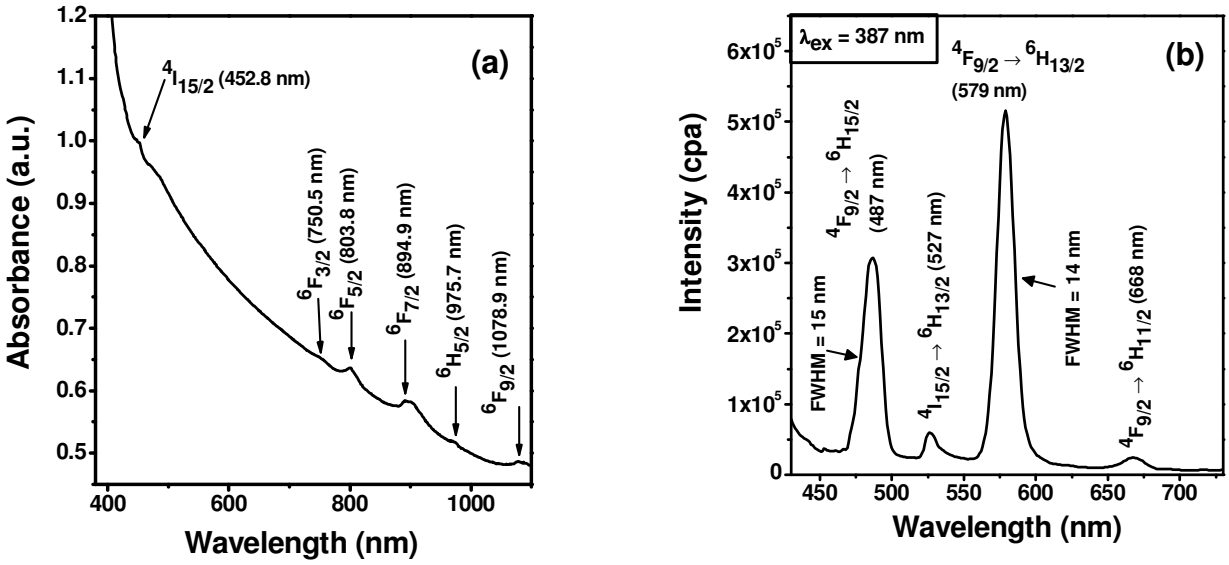

Fig. 5. (a) and (b).

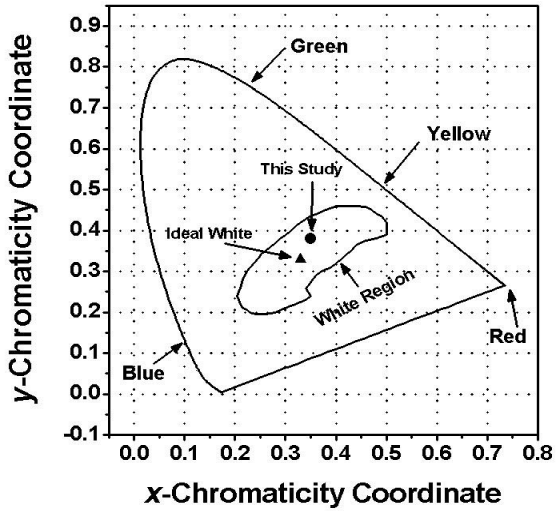

Fig. 5(c).

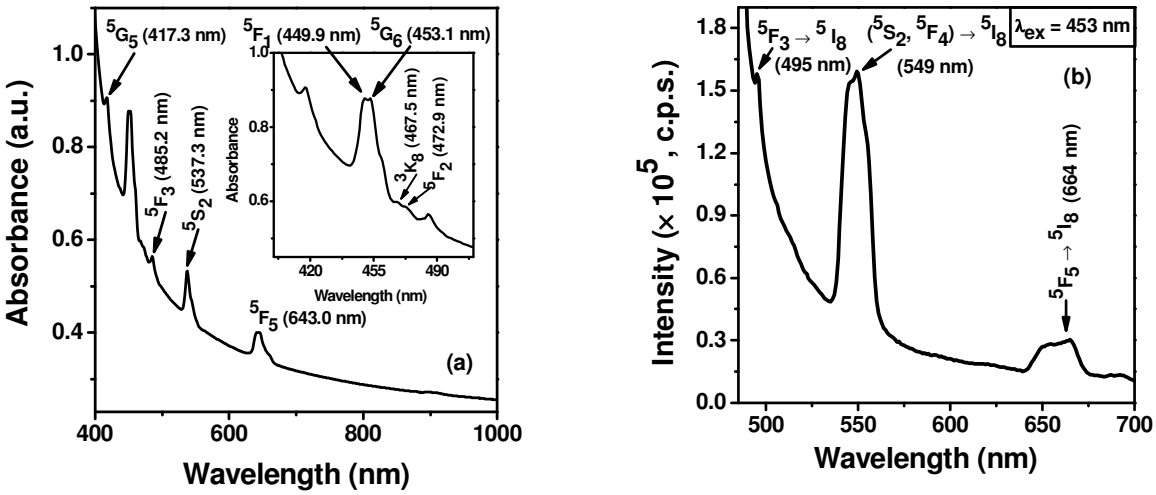

Fig. 6. (a) and (b).

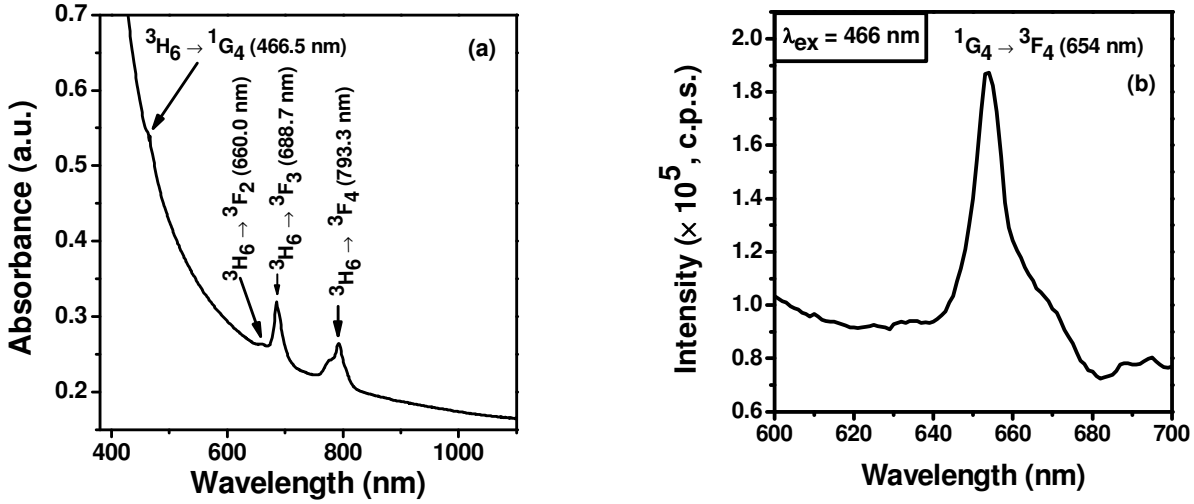

Fig. 7. (a) and (b).

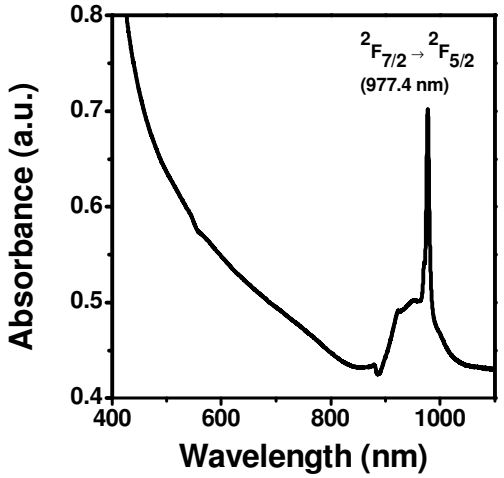
Absorbance (a.u.)
Wavelength (nm)
$^2F_{7/2} \rightarrow {}^2F_{5/2}$
(977.4 nm)
0.8
0.7
0.6
0.5
0.4
400
600
800
1000

Fig. 8.

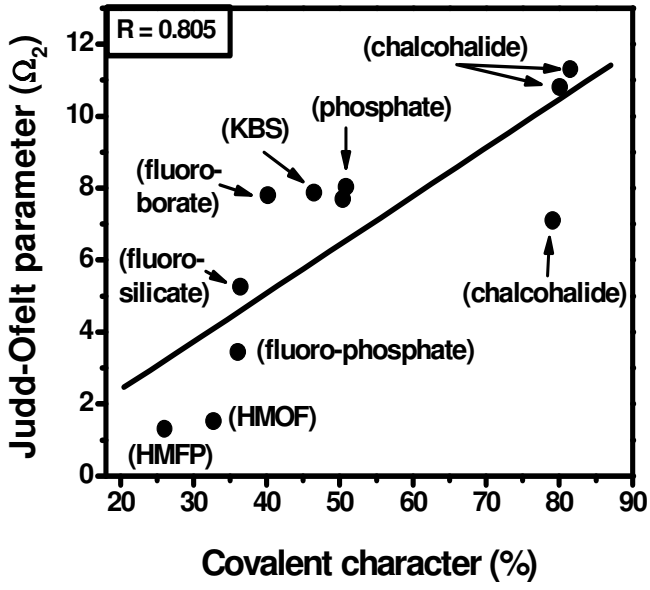
R = 0.805
Judd-Ofelt parameter (Ω_2)
Covalent character (%)
(chalcohalide)
(phosphate)
(KBS)
(fluoro-borate)
(fluoro-silicate)
(chalcohalide)
(fluoro-phosphate)
(HMOF)
(HMFP)
0
2
4
6
8
10
12
20
30
40
50
60
70
80
90

Fig. 9.

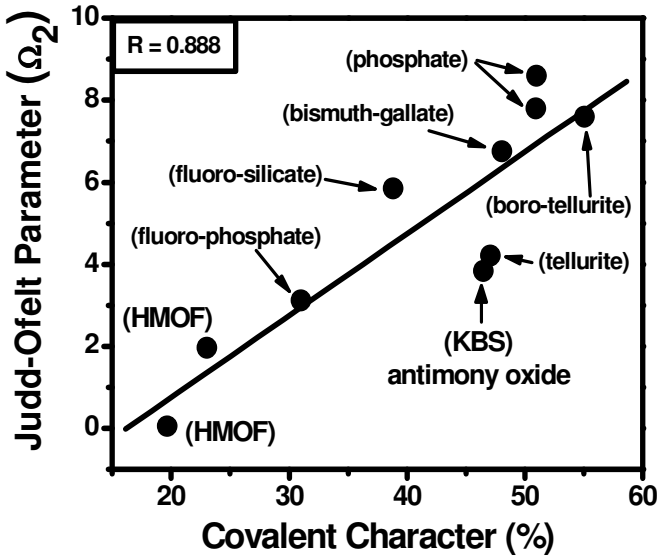
R = 0.888
(phosphate)
(bismuth-gallate)
(fluoro-silicate)
(boro-tellurite)
(fluoro-phosphate)
(tellurite)
(HMOF)
(KBS)
antimony oxide
(HMOF)
Judd-Ofelt Parameter (Ω2)
Covalent Character (%)
0
2
4
6
8
10
20
30
40
50
60

Fig. 10.

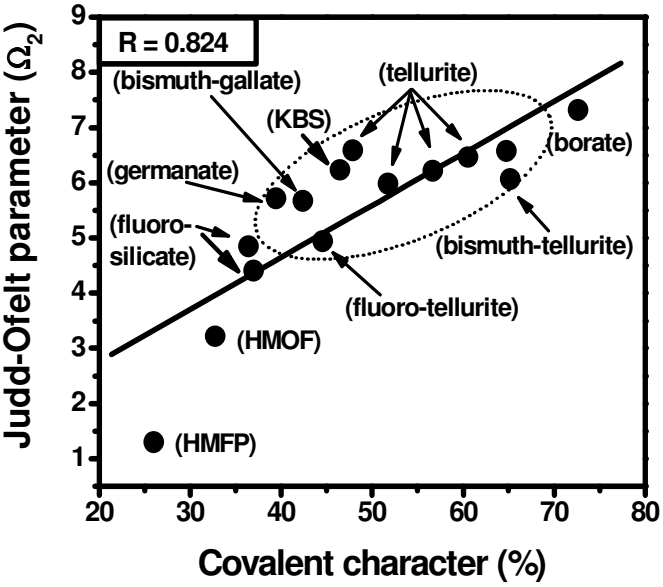
R = 0.824
(bismuth-gallate)
(tellurite)
(KBS)
(borate)
(germanate)
(fluoro-
silicate)
(bismuth-tellurite)
(fluoro-tellurite)
(HMOF)
(HMFP)
Judd-Ofelt parameter (Ω2)
Covalent character (%)
1
2
3
4
5
6
7
8
9
20
30
40
50
60
70
80

Fig. 11.